Calcium channel-coupled transcription factors facilitate direct nuclear signaling

Eshaan R. Rao[1*], Tyler Thaxton[1*], Eric Gama[1], Jack Godfrey[1], Cenfu Wei[1], Qiaoshan Lin[2], Yan Li[2], Daniel Parviz Hejazi Pastor[1], Christian Hansel[3], Xiaofei Du[1#], Christopher M. Gomez[1#]

[1] Department of Neurology, University of Chicago, Chicago, IL 60637, USA

[2] Center for Research Informatics, University of Chicago, IL 60637, USA

[3] Department of Neurobiology, University of Chicago, Chicago, IL 60637, USA

*These authors contributed equally to this work

[#]Correspondence to: feliciad@uchicago.edu, gomez001@uchicago.edu

Summary

VGCCs play crucial roles within the CNS, in maintaining cell excitability, enabling activity-dependent neuronal development, and forming long-term memory by regulating Ca^{2+} influx. The intracellular carboxyl-terminal domains of VGCC α1 subunits help regulate VGCC function. Emerging evidence suggests that some VGCC C-termini have functions independent of channel gating and exist as stable proteins. Here, we demonstrate that all VGCC gene family members express bicistronic mRNA transcripts that produce functionally distinct C-terminal proteins (CTPs) in tandem with full-length VGCC α1 subunits. Two of these CTPs, α1CCT and α1ACT, cycle to and from the nucleus in a Ca^{2+}- and calmodulin-dependent fashion. α1CCT, α1ACT, and α1HCT regulate chromatin accessibility and/or bind directly to genes, regulating gene networks involved in neuronal differentiation and synaptic function in a Ca^{2+}-dependent manner. This study elucidates a conserved process of coordinated protein expression within the VGCC family, coupling the channel function with VGCC C-terminal transcription factors.

Keywords:

Voltage-gated Ca^{2+} channels, bicistronic cellular genes, C-terminal proteins, Ca^{2+} signaling, neuronal differentiation, synaptic function, *CACNA1A, CACNA1C, CACNA1H*, α1ACT, α1CCT, α1HCT, VGCC

40 **Introduction**

41 Calcium (Ca^{2+}) is a ubiquitous second messenger that regulates numerous biological properties
42 and activities throughout eukaryotic cells. Ca^{2+} signaling is especially important in the nervous
43 system, acting both intra- and intercellularly to convey critical information necessary for its
44 proper development and function. One tool within the neuronal Ca^{2+} signaling toolkit is the
45 diverse family of Ca^{2+}-permeable channels present among neuron subtypes, each one having
46 unique gating and transduction pathways. These voltage-gated Ca^{2+} channels (VGCCs) are
47 integral in maintaining neuronal excitability, synaptic transmission, muscle contractility, activity-
48 dependent changes in gene expression, and long-term learning and memory changes within the
49 central nervous system (CNS). Ca^{2+} signaling through VGCCs has also been shown to be
50 critically important for proper migration of neuronal cells, such as granule cells in the
51 cerebellum, neurons in the postnatal olfactory bulb, and interneurons in the cortex (Bortone and
52 Polleux, 2009; Darcy and Isaacson, 2009; Komuro and Rakic, 1996).

53 The main pore-forming alpha 1 (α1) subunits of Ca^{2+} channels comprise a family
54 encoded by ten distinct genes (*CACNA1X*) corresponding to three subfamilies (Ca_v1, Ca_v2, and
55 Ca_v3), and give rise to distinct high-voltage activated/high conductance (L-type, Ca_v1), high-
56 voltage activated/low conductance (Ca_v2) and low-voltage activated/transient (Ca_v3) Ca^{2+}
57 channels. Alpha 1 subunits assemble with accessory subunits and have important interactions
58 via their intracellular C-terminal domains with several intracellular proteins to confer gating
59 properties, mediate signal transduction and facilitate subcellular compartmentalization (Best and
60 Kamp, 2012; Neely and Hidalgo, 2014). Numerous loss- or gain-of-function mutations in each
61 of the α1 subunits have wide- ranging effects on the VGCC gene products and lead to
62 debilitating neurological, neuropsychiatric, muscle, sensory, or cardiac disorders. However, due

63 to their phenotypic and genetic complexity, clear insights into pathogenesis and therapeutic
64 strategies remain elusive for these genetic disorders.

65 Most well-recognized examples of Ca^{2+}-coupled processes represent demonstrable
66 integration between ion channels and separate signaling molecules encoded by distinct genes,
67 such as the Ca^{2+}-dependent enzymes, calmodulin-dependent protein kinase II (CaMKII),
68 calcineurin, and protein kinase C (PKC) (Dolmetsch et al., 2001; Wheeler et al., 1994; Wheeler
69 et al., 2008; Wheeler et al., 2012). The intracellular translocation and activation of certain
70 transcription factors (TFs), including the developmental TFs, NFAT, CREB, and MEF-2, is
71 regulated by highly precise spatial and temporal Ca^{2+} signaling within neurons (Beals et al.,
72 1997; Belfield et al., 2006; Hardingham et al., 2001; Linseman et al., 2003; Mao et al., 1999; Wu
73 et al., 2001).

74 Recent studies have suggested a role for Ca^{2+} channel proteins in a more direct form of
75 nuclear signaling, through the production of Ca^{2+} channel C-terminal proteins (CTPs) (Bannister
76 et al., 2013; Du et al., 2013; Gomez-Ospina et al., 2006; Yang et al., 2022). The origin and
77 function of these CTPs has not been definitively ascertained, although our previous findings
78 suggest that, for at least some cases, *e.g., CACNA1C , CACNA1A,* and *CACNA1H,* encoding
79 α1C, α1A, and α1H respectively, this may represent a form of *genetic coupling* to neuronal Ca^{2+}
80 signaling molecules (Du et al., 2019), as has been recognized for several other mammalian genes
81 (Karginov et al., 2017). The *CACNA1A* mRNA, for example, encodes the α1A Ca^{2+} channel
82 subunit of the P/Q-type VGCC $Ca_v2.1$, as well as a second protein, a newly recognized TF,
83 termed α1ACT, which activates an ensemble of genes that are critical for early cerebellar
84 development. Mutations in *CACNA1A* have also been associated with cerebellar developmental
85 disorders. Pathological expansion of a glutamine repeat tract in the α1ACT protein abolishes

86 normal TF activity and mediates the progressive disease spinocerebellar ataxia type 6 (Du et al.,
87 2013; Du et al., 2019). Furthermore, some mutations in the *CACNA1C* gene, encoding the
88 $Ca_v1.2$, α1C subunit, as well as a C-terminal TF, lead to cardiac defects, arrhythmias, and
89 profound neurodevelopmental phenotypes (Cipriano et al., 2024; Gomez-Ospina et al., 2013;
90 Gomez-Ospina et al., 2006; Rodan et al., 2021).

91 In this study, we formally explored the molecular basis, physiological control, and
92 function of CTP expression for the VGCC gene family. Our findings demonstrate that all ten
93 neuronal VGCC genes appear to express α1 Ca^{2+} channel CTPs by an alternative translation
94 process, with these ten CTPs being distributed in both cytoplasm and nucleus. Detailed
95 examination of the mRNA transcripts from the three branches of the VGCC family encoding
96 α1C, α1A, and α1H revealed that the CTPs, referred to here as α1ACT, α1CCT and α1HCT,
97 respectively, are generated from overlapping cistrons through a non-canonical, cap-independent
98 mechanism. For at least two of these CTPs, α1ACT and α1CCT, nuclear translocation is
99 functionally coupled to Ca^{2+}-calmodulin signaling through ion channels in primary neurons.
100 Furthermore, we found that in human neural progenitor cells (hNPCs), α1CCT, α1ACT and
101 α1HCT, each interact with DNA to regulate the expression of an array of genes crucial for proper
102 neuronal development/differentiation and synapse formation. Interestingly, these functions are
103 Ca^{2+}-dependent and involve specific TF motif-binding in response to depolarization. Finally,
104 when tested *in vivo*, α1CCT restores the disrupted gene expression program in a conditional
105 *CACNA1C* knockout mouse.

106 These findings reveal a conserved, coordinated strategy of genetically and
107 physiologically coupled signals for modulating gene expression among these neuronal VGCC

108 genes. Dysregulation of this efficient strategy may explain the widespread, pleiotropic
109 phenotypes observed in disorders related to VGCC gene mutations.

110

111 **Results:**

112 **VGCC genes encode two distinct proteins from overlapping cistrons**

113 Based on our findings of dual protein expression by the three VGCC genes, *CACNA1C,*
114 *CACNA1A,* and *CACNA1H,* we hypothesized that dual protein expression was common to the
115 remaining members of the VGCC gene family (Du et al., 2019). To test this for the remaining
116 seven VGCC genes, *CACNA1S* (*C*a_v1.1), *CACNA1D* (Ca_v1.3), *CACNA1F* (Ca_v1.4), *CACNA1B*
117 (Ca_v2.2), *CACNA1E* (Ca_v2.3), *CACNA1G* (Ca_v3.1), and *CACNA1I* (Ca_v3.3) (Supplementary
118 Table 1), we transfected HEK293T cells with cDNAs expressing each of the ten VGCC α1
119 subunits extended at the C-terminus with a 3xFLAG epitope tag. The cDNAs corresponding to
120 each of the VGCC genes expressed ~250 kDa proteins detected with the anti-FLAG antibody
121 (Figure 1D-F). In addition, these cells expressed smaller proteins that were also reactive with
122 FLAG antibody, ranging in size from 37 - 85 kDa (Figure 1D-F; Supplementary Table 1).
123 Previous expression studies *in vitro* have attributed the presence of smaller Ca^{2+} channel
124 fragments to proteolytic cleavage or the presence of cryptic intragenic promoters (Andrade et al.,
125 2007; Ge et al., 2013; Gomez-Ospina et al., 2013; Gomez-Ospina et al., 2006). To demonstrate
126 that the expression of smaller CTPs was independent of the full-length Ca^{2+} channel proteins, we
127 inserted premature termination codons upstream of the putative CTP start sites ($CACNA1X_{Stop}$),
128 as predicted by size estimates (Figure 1A-C). In some cases, to abolish initiation at secondary
129 methionine codons, additional stop codons were inserted. In all cases, expression of the full-

130 length, FLAG-tagged α1 subunits was abolished and, as we had observed with *CACNA1C,*
131 *CACNA1A* and *CACNA1H*, expression of the smaller 37 - 85 kDa CTPs persisted for *CACNA1S,*
132 *CACNA1D, CACNA1F, CACNA1B, CACNA1E, CACNA1G,* and *CACNA1I* (Figure 1D-F). These
133 results indicate that the CTPs are not the products of proteolytic cleavage of the full-length α1
134 subunits, and that expression of the CTPs in the VGCC gene family does not require expression
135 of the full-length Ca^{2+} channel protein.

136

137 **mRNA segments of *CACNA1C, CACNA1A,* and *CACNA1H* drive internal, cap-independent**
138 **translation of CTPs**

139 We previously used protein truncation and point mutation experiments, as well as mass
140 spectrometry, to identify the start sites for CTPs expressed by the neuronal VGCC genes,
141 *CACNA1C*, *CACNA1A*, and *CACNA1H,* belonging to *three distinct VGCC subfamilies* and
142 encoding α1 subunits, α1A ($Ca_v2.1$), α1C ($Ca_v1.2$), and α1H ($Ca_v3.2$), respectively (see Figure
143 1A) (Du et al., 2013; Du et al., 2019). Their corresponding CTPs, α1ACT (NM_001127222.1:
144 AUG 6114nt), α1CCT (NM_199460.3: AUG 5469nt), and α1HCT (NM_021098.2: AUG
145 6045nt), designated according to the α1 subunit of origin, correspond to 70 - 75 kDa proteins
146 seen in western blots of mouse forebrain tissue probed with C-terminus-directed antisera (Du et
147 al., 2019). To preclude the possibility that these smaller gene products arise due to the presence
148 of cryptic promoters or alternative splicing, we used cellular transfections of *in vitro*-transcribed
149 mRNAs. We transfected HEK293T cells with mature, polyA-tailed mRNAs encoding the three
150 full-length VGCC α1 subunits extended at the C-terminus with a 3xFLAG epitope tag. The
151 mRNAs were capped on the 5' end, either with a canonical m7G cap (G-capped mRNA),

allowing for initiation of translation, or with a modified 5' cap consisting of m7G(5')ppp(5') A cap (A-capped mRNA). The modified A-cap inhibits binding of the initiation complex and the initiation of cap-dependent translation of the full-length α1 subunits, although may also reduce mRNA stability. In Western blots probed with an anti-FLAG antibody, we observed that G-capped mRNAs from *CACNA1C, CACNA1A,* and *CACNA1H* expressed the full-length α1 VGCC subunits of ~250 kDa in size, as well as the smaller CTPs, α1CCT (~70 kDa), α1ACT (~75 kDa), and α1HCT (~70 kDa) (Figure S1A-C). Interestingly, in cells transfected with A-capped mRNAs, the full-length α1 subunit expression was abolished while the CTPs persisted, although with reduced CTP protein expression compared to that observed with G-capped mRNAs (Figure S1A-C). We used FLAG-specific qPCR primers to confirm that the reduced CTP expression corresponded to reduced levels of A-capped VGCC mRNA, consistent with a lower stability of A-capped mRNAs, rather than an effect on translation initiation of the CTPs (Figure S1D-F). To interfere with translation of the full-length protein, we transcribed mRNAs from the cDNA templates for transfection into cells after either of two additional modifications: 1) insertion of premature termination codons between the initiation codon of the full-length α1 subunit and the putative start sites of the CTPs {$CACNA1C_{stop}$ (1264nt, 3607-3609nt); $CACNA1A_{stop}$ (5791nt); $CACNA1H_{stop}$ (3939 and 3941nt, 3948and 3950nt)}, or 2) insertion of sequences that generate large RNA hairpins at the 5' end of the coding sequence, designed to impede ribosomal elongation. The RNA hairpin, with a $-\Delta G$ of -50, which is known to significantly reduce cap-dependent translation, was inserted 28 nt downstream of the T7 site in the plasmid containing the full-length VGCC open reading frame (Godfrey et al., 2022). We observed that full-length α1 subunits were not generated from mRNAs bearing either the premature termination codons or inserted hairpins, while FLAG-tagged CTPs were readily

175 detected (Figure S1A-C), suggesting that they are generated by internal ribosomal entry, rather
176 than a process such as ribosomal slipping or shunting.

177 To further verify that α1CCT and α1HCT are generated from the same mRNAs as their
178 respective VGCC subunits, we transfected HEK293T stable cell lines expressing full-length
179 *CACNA1C* or *CACNA1H* with siRNAs directed towards the 5' ends of the *CACNA1C* or
180 *CACNA1H* genes. These siRNAs abolished expression of the full-length α1 subunits as well as
181 the secondary proteins, presumably through the RNA Induced Silencing Complex (RISC),
182 suggesting that both are expressed from the same mRNA (Figure S1G and H). We previously
183 reported a similar effect, induced by two distinct microRNAs, miR-711 and miR-4786-3p,
184 directed at sequences upstream of α1ACT in cells transfected with *CACNA1A*-expressing
185 constructs, leading to elimination of both the full length α1A and α1ACT proteins (Miyazaki et
186 al., 2016).

187 Using an M-fold based algorithm of RNA folding on *CACNA1C* and *CACNA1H* VGCC
188 gene transcripts, we predicted that the regions directly upstream of the α1CCT and α1HCT start
189 sites form a series of highly stable stem-loop structures that could represent regions of binding
190 by canonical translation initiation factors, as shown previously for *CACNA1A* (Du et al., 2013;
191 Du et al., 2019). To test for the capacity of RNA segments within these regions to initiate
192 protein translation, we inserted 1000 base pair (bp) segments of DNA from the regions directly
193 upstream of the predicted α1CCT and α1HCT start sites into the bicistronic reporter vector pRF
194 (*Renilla* luciferase, R-luc, and firefly luciferase, F-luc), and transfected these reporters into
195 HEK293T cells. The coding region for R-luc is followed by a termination codon, therefore a
196 relative increase in F-luc activity in cell lysates indicates that the inserted RNA segment can
197 enable re-initiation of translation in a cap-independent manner (Spriggs et al., 2009). The 1000

198 bp segment insertions from the *CACNA1C* and *CACNA1H* genes led to significant increases in F-
199 luc activity, 28.27±2.37 fold ($p < 0.0001$) and 17.38±0.14 fold ($p < 0.0001$) respectively,
200 compared to empty pRF vector control (Figure S1I). These results suggest that, as with α1ACT,
201 expression of α1CCT and α1HCT is driven by the presence of cellular IRES-like structures
202 within the *CACNA1C* and *CACNA1H* coding regions, respectively.

203 Taken together, these studies indicate that the VGCC genes and their mRNAs are
204 bicistronic, each producing the full-length α1 subunits in addition to a smaller CTP. Whereas the
205 full-length α1 subunits are generated by canonical cap-dependent translation, the three CTPs are
206 generated in the absence of cap-dependent translation.

207

208 **Nuclear Distribution of VGCC CTPs**

209 α1ACT translocates to the nucleus in transfected cells (HEK293T, NIH3T3, and cerebellar
210 granule cells), and is detected in cerebellar Purkinje cell nuclei (Du et al., 2013; Du et al., 2019;
211 Kordasiewicz et al., 2006). To test the subcellular distribution of the other nine full-length α1
212 subunits and the CTP protein products, we transfected HEK293T cells with plasmids expressing
213 each of the C-terminal 3xFLAG-tagged α1 subunits used in Figure 1, with and without inserted
214 premature stop codons, and immunolocalized the proteins using anti-3xFLAG antibody (red
215 fluorescence) and confocal microscopy. Immunolabeling of the cell membrane and cytoplasm
216 was readily detectable in cells transfected with each of the intact 3xFLAG-tagged VGCC
217 subunits (Figure 1). Interestingly, in addition to the labeling detected in the cytoplasm and
218 membrane, nuclear staining in the same cell nucleus could be detected in cells expressing α1S,
219 α1C, α1D, α1A, α1B, α1E, α1H, and α1I, while in α1F- and α1G-expressing cells only

220 cytoplasmic fluorescence was detected. Since the α1 subunits are transmembrane proteins that
221 cannot translocate to the nucleus, it is likely that proteins imaged in the nucleus are from the C-
222 terminus. Notably, nuclear labeling was detected in cells transfected with all ten VGCC-
223 expressing plasmids, including α1F and α1G, bearing premature stop codons (*CACNA1X*$_{Stop}$)
224 (Figure 1G-I). These constructs express only 3xFLAG-tagged CTPs, while expression of the
225 full-length α1 subunit is abolished (Figure 1D-F). Also, in all cases except *CACNA1S,* the
226 proportion of cells with labelling in the cytoplasm and membrane was decreased, while the
227 proportion of cells with labeling in the nuclei was significantly increased when transfected with
228 *CACNA1X*$_{Stop}$ (Supplementary Table 2). For example, for *CACNA1A*, fluorescent labelling in the
229 nucleus was greatly increased, from an average of 63.43 ± 6.3% to 100 ± 0% ($p < .05$) when cells
230 were transfected with intact *CACNA1A* compared with *CACNA1A*$_{Stop}$, suggesting an
231 accumulation of C-terminal 3xFLAG fusion protein. No cytoplasmic labeling was detected in
232 cells transfected with *CACNA1A*$_{Stop}$ (Figure 1H, Supplementary Table 2). Similarly, for
233 *CACNA1C*, nuclear fluorescence increased from an average of 13.66 ± 4.13% to 69.75 ± 16.36
234 % ($p < .05$) when cells were transfected with *CACNA1C* compared with *CACNA1C*$_{Stop}$, again
235 suggesting an accumulation of C-terminal 3xFLAG fusion protein. Cytoplasmic labeling reduced
236 from an average of 86.34 ± 4.13% to 30.25% ± 16.35 % ($p < .05$) (Figure 1G, Supplementary
237 Table 2). For *CACNA1H*, nuclear labeling was also greatly increased, from an average of 3.42 ±
238 2.15% to 37.29 ± 7.07 % ($p < .05$), when cells were transfected with *CACNA1H* compared with
239 *CACNA1H*$_{Stop}$, while cytoplasmic labeling reduced from an average of 96.57 ± 2.15% to 62.71%
240 ± 7.07% ($p < .05$) (Figure 1I, Supplementary Table 2). Lastly, no nuclear labeling was detected
241 in cells transfected with intact *CACNA1F*- and *CACNA1G*-expressing plasmids. However, for
242 *CACNA1F*$_{Stop}$, 62.79 ± 10.18% ($p < .05$) of the labeling remained in the cytoplasm, while cells

243 with nuclear labeling increased to 37.21 ± 10.18% (Figure 1G, Supplementary Table 2). Cells
244 transfected with *CACNA1G*$_{Stop}$ predominantly exhibited cytoplasmic labeling, with only a few
245 cells having nuclear labeling (Figure 1I, Supplementary Table 2). In summary, increases in
246 nuclear labeling were seen in cells expressing CTPs expressed by all ten VGCC constructs.
247 Together, these findings suggest that the CTPs encoded by these VGCC transcripts are present
248 naturally in the cytoplasm and can translocate to the nucleus.

249

250 **Subcellular localization of α1CCT and α1ACT is coupled to neuronal Ca^{2+} signaling in**
251 **primary cortical neurons**

252 Given that the native CTPs are encoded by the same transcripts as the VGCC α1 subunits, and
253 CTPs are present both in cytoplasmic and nuclear compartments, we tested whether changes in
254 intracellular Ca^{2+} concentration, in a neuronal context, would influence CTP subcellular
255 localization. To elicit increases in intracellular Ca^{2+}, we treated primary neurons transfected with
256 CTP-expressing constructs with either potassium chloride (KCl), glutamate (Glu), or the Ca^{2+}
257 ionophore A23187. Exposure to increased extracellular KCl or Glu results in cellular
258 depolarization followed by Ca^{2+} influx, partially mediated through L-type VGCCs (Sharma et
259 al., 2008). Glu, an excitatory neurotransmitter, additionally activates glutamate-dependent cation
260 channels (Zhang et al., 2019). A23187 is an ionophore that is highly selective for Ca^{2+} and results
261 in rapid and robust Ca^{2+} influx in intact cells (Mattson et al., 1993; Mattson et al., 1991; Xie et
262 al., 1996). We first studied the subcellular distribution of α1CCT, α1ACT, and α1HCT in mature
263 primary rat cortical neurons, via fixed-cell immunocytochemistry following the induction of
264 intracellular Ca^{2+} changes. We transfected neurons at DIV 15-17 (days in vitro) with vectors
265 expressing 3xFLAG-tagged VGCC CTP mRNAs in culture, and manipulated intracellular Ca^{2+}

266 concentrations with KCl (20 mM), Glu (100 μM), or A23187 (5 μM). Each treatment was
267 evaluated in the presence and absence of the intracellular Ca^{2+} chelator, BAPTA-AM (40 μM).
268 Neurons were treated for five minutes, after which they were fixed, and the cytoplasmic and
269 nuclear 3xFLAG fluorescence signal for each CTP was quantified.

270 In untreated control neurons expressing α1CCT, the mean nuclear-to-cytoplasmic (N-C)
271 ratio was 1.736±0.05. After treatment with 20 mM KCl, the N-C ratio was 1.955±0.07, which is
272 slightly increased from the control ($p < 0.05$ vs control) (Figure 2A-C). However, exposure to
273 Glu resulted in a significantly higher N-C ratio of 2.370±0.08 ($p<0.0001$ vs control) (Figure 2C).
274 A23187 had the most pronounced effect on α1CCT nuclear-cytoplasmic localization, with an N-
275 C ratio of 2.843±0.17 ($p< 0.0001$ vs control) (Figure 2C). Importantly, co-treatment of
276 transfected neurons with the Ca^{2+} chelator BAPTA-AM during exposure to KCl, Glu or A23187
277 prevented the shift in N-C ratio, which was measured at 1.766±0.06 for KCl/BAPTA ($p = 0.9733$
278 vs control) and 1.861±0.09 for Glu/BAPTA ($p = 0.2972$ vs control), and was further reduced to
279 1.339±0.06 for A23187/BAPTA ($p < 0.0001$ vs control) (Figure 2B and C). These results
280 indicate the importance of Ca^{2+} in the translocation of α1CCT.

281 For α1ACT, activity-mimicking stimuli had the opposite effect on subcellular
282 localization. In untreated control neurons expressing α1ACT, the N-C ratio was 2.88±0.10.
283 After treatment with 20 mM KCl, the N-C ratio was reduced to 2.33±0.14 ($p < 0.001$ vs control)
284 (Figure 2D-F). Treatment with Glu led to a similar reduction in the N-C ratio to 2.32±0.13 ($p <$
285 0.01 vs control), and A23187 treatment led an N-C ratio of 2.42±0.17 ($p < 0.05$ vs control)
286 (Figure 2F). Moreover, the activity-induced reduction in the N-C ratio of α1ACT was prevented
287 or reversed by Ca^{2+}chelation with BAPTA-AM (Figure 2E and F), again pointing to the
288 importance of Ca^{2+} in the translocation of α1ACT. Interestingly, none of these brief stimuli had a

289 significant effect on the subcellular localization of α1HCT (Figure S2A - C), suggesting that the
290 localization and translocation of the *CACNA1H*-derived CTP may not be regulated by Ca^{2+}
291 signaling under the conditions or time course of this study. In summary, these observations
292 demonstrate that the subcellular translocation of α1CCT and α1ACT shifts in response to
293 activity-mimicking stimuli, suggesting Ca^{2+}-dependence.

294

295 **Real-time nuclear translocation of α1CCT and α1ACT parallels Ca^{2+} signaling in primary**
296 **cortical neurons**

297 To visualize the effects of elevated intracellular Ca^{2+} on nuclear-cytoplasmic translocation of
298 α1CCT and α1ACT in real-time, we replaced the C-terminal 3xFLAG tag with Emerald GFP
299 (EmGFP) and monitored CTP localization and translocation in response to stimuli using live-cell
300 confocal microscopy. Simultaneously, we used the high-affinity Ca^{2+} indicator, Rhod-2 AM, to
301 follow intracellular Ca^{2+} levels. Primary neurons were infected with Adeno-associated virus
302 (AAV9) expressing either α1CCT-EmGFP, α1ACT-EmGFP, or α1HCT-EmGFP, or with control
303 empty vector expressing EmGFP (EV-EmGFP) (all driven by the EF1α promoter). Five days
304 post-infection, neurons were loaded with Rhod-2 AM and then treated with 4-methoxy-7-
305 nitroindolinyl (MNI) L-glutamate, a form of caged glutamate (Glu). Neuronal nuclei were
306 identified by the fluorescent nuclear marker DRAQ5. Uncaging of Glu extracellularly around
307 the basal dendrites and cell bodies of cortical pyramidal neurons resulted in reproducible, high-
308 quality Ca^{2+} spikes within the targeted subset of neurons, as judged by Rhod-2 AM (red
309 fluorescence), and these Ca^{2+} spikes frequently propagated to the nucleus (Figure S2D-F). For
310 cells exhibiting Ca^{2+} spikes, the translocation of CTPs between nuclear and cytoplasmic
311 compartments was recorded over a 10-minute observation period after Glu uncaging. The extent

312 of CTP translocation into the nucleus was compared with the behavior of EV-EmGFP (and
313 untreated CTPs-EmGFP). For α1CCT-expressing cells, Glu uncaging resulted in an *increase* in
314 nuclear fluorescence of 20.95±1.5% ($p<0.0001$ vs untreated) over 10 minutes (Figure 2G-I,
315 Supplementary Video 1 and 2). In contrast, for α1ACT-expressing cells, Glu stimulation over
316 the same period led to a *decrease* in nuclear fluorescence of 10.73±1.6% ($p<0.0001$ vs untreated)
317 (Figure 2G-I, Supplementary Video 1 and 3). Finally, while α1HCT showed no significant
318 movement over this interval, it tended to enter the nucleus at a slower rate following intracellular
319 Ca^{2+} spikes (Figure 2H and I, Supplementary Video 1 and 3). These results are consistent with
320 our findings in fixed primary neurons using Glu stimuli and suggest that the translocation of
321 α1CCT and α1ACT is dynamically coupled to Ca^{2+} levels.

322

323 **Active nuclear translocation of α1CCT and α1ACT requires Ca^{2+} signaling through**
324 **VGCCs and NMDA receptors**

325 To explore the sources of Ca^{2+} involved in mediating nuclear translocation of the CTPs, we
326 compared the effects of distinct ion channel and receptor antagonists (Supplementary Table 3).
327 To determine whether Ca^{2+} entry through α1C/Ca_v1.2, α1A/Ca_v2.1, or α1H/Ca_v3.2 was
328 necessary for the subsequent translocation of α1CCT or α1ACT (Adams et al., 1990; Follesa and
329 Ticku, 1996; Hagenston et al., 2009; Kraus et al., 2010; Ruiz et al., 2009; Weiss et al., 1990), we
330 loaded primary cortical neurons, infected with AAV9 expressing α1CCT-EmGFP or α1ACT-
331 EmGFP, with blockers specific for each VGCC subtype, and then stimulated these neurons by
332 Glu uncaging. Compared to Glu uncaging alone, α1CCT nuclear translocation was decreased by
333 Ca_v2.1 blockade (500 nM ω-agatoxin; -7.14 ± 0.021%, $p = 0.0012$) and by Ca_v3.2 blockade (100
334 μM TTA-A2; -5.53 ± 0.020%, $p = 0.0071$) (Supplementary Table 4). However, the Ca_v1.2

335 blocker, nifedipine (10 μM), had the most prominent effect, reducing α1CCT nuclear entry when
336 compared to Glu uncaging alone (-15.24 ± 0.014%, $p < 0.0001$), suggesting that Ca^{2+} signaling
337 through L-type VGCCs plays a prominent role in α1CCT nuclear translocation (Figure 3B-C).
338 To determine whether Ca^{2+} entry through glutamate-binding N-methyl-D-aspartate (NMDA)
339 receptors contributed to α1CCT translocation, we applied the NMDA receptor antagonist, AP5
340 (100 μM). α1CCT nuclear entry with NMDA receptor blockade was reduced when compared to
341 Glu uncaging alone (-6.95±0.014%, $p < 0.0001$), although to a lesser extent than was observed
342 for $Ca_v1.2$ blockade via nifedipine (Figure 3B-C). These results indicate that Ca^{2+} influx through
343 either L-type VGCCs or NMDA channels may facilitate α1CCT nuclear translocation.

344 In neurons infected with AAV9 expressing α1ACT-EmGFP, translocation of α1ACT out
345 of the nucleus was *unperturbed* by the presence of a VGCC blocker: 10 μM nifedipine (+0.7 ±
346 0.020%, $p = 0.7211$), 500 nM ω-agatoxin (1.94 ± 0.021%, $p = 0.3551$), or 100 μM TTA-A2
347 (1.41 ± 0.020%, $p = 0.4910$) (Supplementary Table 3). To identify the source of the Ca^{2+}
348 responsible for α1ACT nuclear export, we used several additional antagonists in tandem with
349 Glu uncaging. To investigate the role of store-operated Ca^{2+}, we loaded α1ACT-EmGFP-
350 expressing neurons with the IP3 antagonist 2-APB (50 μM) and ryanodine (100 μM), prior to
351 Glu uncaging. α1ACT nuclear export was unperturbed following antagonism of intracellular
352 Ca^{2+} store release via 2-APB and ryanodine (2.76 ± 0.018%, $p = 0.1293$ vs Glu alone)
353 (Supplementary Table 3). However, when we exposed α1ACT-EmGFP-expressing neurons to
354 AP5, Glu-induced α1ACT-EmGFP translocation out of the nucleus was reduced to - 4.67 ±
355 0.038%, compared with 10.73 ± 1.6% in the absence of AP5 ($p < 0.01$) (Figure 3D-E). These
356 results suggest that Ca^{2+} entry through NMDA receptors plays a prominent role in triggering
357 translocation of α1ACT from the nucleus.

358 Taken together, our results indicate that α1ACT and α1CCT, the CTPs encoded by
359 overlapping cistrons in the mRNAs expressing α1A and α1C, respectively, are sensitive to
360 cytoplasmic Ca^{2+} levels, and undergo dynamic nuclear-cytoplasmic shuttling within neurons in
361 response to physiological shifts in Ca^{2+} resulting from influx through different Ca^{2+}-permeable
362 channels.

363

364 **Calcium-dependent nuclear translocation of α1CCT and α1ACT acts through calmodulin**

365 The Ca^{2+}-binding protein, calmodulin, serves as the primary intracellular receptor for Ca^{2+} and
366 facilitates Ca^{2+}-dependent signaling mechanisms in neurons (Chemin et al., 2017; Deisseroth et
367 al., 1998; Dolmetsch et al., 2001). To test whether calmodulin affects CTP nuclear transport, we
368 used the cell-permeant calmodulin inhibitor, W-7 hydrochloride (W-7), in primary cortical
369 neurons transfected with GFP-tagged CTPs. W-7 reduced activity-induced α1CCT nuclear entry
370 to 7.25±0.5%, compared with 18.34±1.5% for Glu treatment only ($p<0.0001$) (Figure 3B-C).
371 Similarly, W-7 reduced activity-induced α1ACT nuclear export to 5.76±0.9%, compared with -
372 10.73±1.6% for Glu treatment only ($p = 0.0412$) (Figure 3D-E).

373 Given the effect of W-7 on Ca^{2+}-mediated nuclear and cytoplasmic translocation of
374 α1ACT and α1CCT, we investigated whether there is a direct interaction between calmodulin
375 and the CTPs. We exposed lysates from HEK293T cells expressing 3xFLAG-tagged
376 α1CCT, α1ACT, or α1HCT, to Sepharose beads, either unconjugated or conjugated to
377 calmodulin, and subjected precipitates to SDS-PAGE and immunoblotting. Figure 3F shows that
378 Sepharose-calmodulin was able to precipitate 3xFLAG-tagged α1CCT (70 kDa) and α1ACT
379 (75 kDa), although no signal was seen with lysates from cells expressing α1HCT or with

380 Sepharose beads alone. These results suggest that the Ca^{2+}-dependent nuclear-cytoplasmic
381 translocation of α1CCT and α1ACT requires the participation of calmodulin.

382

383 **VGCC CTPs have restricted mobility within the nucleus of cultured primary neurons**

384 Although we observed a fraction of the CTPs to cycle across the nuclear membrane, we
385 wondered whether they also exhibited restricted mobility within the nucleus, through potential
386 interactions with DNA, as described with some TFs (Goldstein and Hager, 2018; Govindaraj et
387 al., 2019). To test this, we performed fluorescence recovery after photobleaching (FRAP)
388 (Leake, 2018; Stenoien et al., 2001). We infected cultured primary neurons at DIV10 with AAV9
389 virus expressing EV-EmGFP, α1CCT-EmGFP, α1ACT-EmGFP, or α1HCT-EmGFP. Images
390 were taken at DIV 15-17 following a brief (100 ms), high-intensity pulse of light to bleach the
391 nucleus of imaged cells. We measured the recovery of fluorescence signal for 10 minutes post-
392 bleach. Compared with EV-EmGFP alone, α1CCT-EmGFP, α1ACT-EmGFP, and α1HCT-
393 EmGFP all exhibited significantly slower recovery times (EV $t_{1/2} = 185 \pm 24$s, α1CCT $t_{1/2} =$
394 532 ± 50s, α1ACT $t_{1/2} = 557 \pm 55$s, α1HCT $t_{1/2} = 996 \pm 55$s) (Figure S3A). Additionally,
395 quantification of the mobile fraction (MF) shows significantly lower MFs for α1CCT-EmGFP
396 (46.7±15.9%, $p < 0.01$ vs. EmGFP), α1ACT-EmGFP (28.5±1.0%, $p < 0.0001$ vs. EmGFP), and
397 α1HCT-EmGFP (32.5±5.3%, $p < 0.0001$ vs. EmGFP), compared to EmGFP (58.0±2.5%) (Figure
398 S3B). These findings demonstrate that α1CCT-EmGFP, α1ACT-EmGFP, and α1HCT-EmGFP
399 have a reduced nuclear mobile pool available for active nuclear transport compared to EmGFP,
400 suggesting potential interactions with chromatin by all three CTPs.

401

402 **VGCC CTPs bind to genomic DNA in hNPCs in a calcium-dependent manner**

403 We looked for further evidence of direct interactions of CTPs with chromatin using the
404 CUT&RUN-seq technique (Cleavage Under Targets & Release Using Nuclease, followed by
405 high throughput sequencing). We performed the genomic binding studies in hNPC stable lines
406 expressing either α1CCT, α1ACT, or α1HCT. The three 3xFLAG-tagged CTPs and their DNA
407 complexes were each isolated from these hNPC stable lines, following binding by an antibody
408 against 3xFLAG, H3K4me3 or IgG, and excision by in protein A-protein G-micrococcal
409 nuclease (pAG-MNase). These experiments were performed under basal and depolarizing
410 conditions, the latter induced by 20 mM KCl to elevate intracellular Ca^{2+} levels. Intracellular
411 Ca^{2+} changes were confirmed using the Ca^{2+} indicator Rhod-2 AM, which showed a
412 sustained 1.81± 0.67-fold change ($p<0.003$) in control hNPCs (Figure S4A) and stable nuclear
413 CTP signals after 20 minutes of incubation. The genomic binding profiles revealed that, in either
414 depolarized or resting conditions, α1CCT, α1ACT, and α1HCT were highly enriched within
415 ±3000 bp of annotated transcription start sites (TSSs) (Figure 4A). In particular, α1ACT and
416 α1HCT exhibited enhanced binding near TSS in depolarized cells compared to resting cells
417 (Figure 4A). Binding at TSS was prominently detected in H3K4me3 antibody-isolated samples
418 across all three CTP-expressing hNPC lines (Figure S4B), with 207 binding sites overlapping
419 among the three CTPs (Figure S4C). In contrast, no more than one overlap in binding sites was
420 observed among the CTP-specific samples isolated by the 3xFLAG antibody across three CTPs
421 in either condition (Figure 4C). Comparing binding sites under depolarized and resting
422 conditions in all three CTP expressing hNPCs, a more than 75% overlap was observed in
423 H3K4me3 antibody-isolated samples (Figure S4D). However, the overlap in binding sites was
424 significantly lower for 3xFLAG antibody isolated samples: α1CCT (5.93%), α1ACT (19.9%),

425 and α1HCT (6.1%), respectively, suggesting that cell depolarization leads to a significant and
426 specific change in the gene binding profiles of α1CCT, α1ACT, and α1HCT (Figure 4B).

427 Collectively, these observations indicate that α1CCT, α1ACT, and α1HCT exhibit
428 physiological DNA binding properties near TSS regions and have distinct binding profiles.
429 Moreover, these profiles are significantly altered under cell-depolarizing conditions. Our
430 findings strongly support the notion that all three CTPs function as classical TFs and are
431 involved in the Ca^{2+}-dependent transcriptional regulation of specific target genes in hNPCs.

432

433 **VGCC CTPs increase chromatin accessibility in hNPCs**

434 To assess potential global transcriptional alterations mediated by α1CCT, α1ACT, and α1HCT,
435 we probed the chromatin accessibility changes, using ATAC-seq in the stable hNPC lines
436 expressing either α1CCT, α1ACT, α1HCT, or empty pLXV vector as control. The specific
437 chromatin binding sites associated with α1CCT, α1ACT, and α1HCT were identified by
438 comparing the patterns of accessibility seen in the presence and absence of CTPs. Given that
439 nuclear translocation of α1CCT and α1ACT, and the gene binding patterns of all three CTPs, are
440 affected by intracellular Ca^{2+} levels, we performed ATAC-seq on the hNPC lines in the presence
441 and absence of 20mM KCl. All three CTPs modify chromatin accessibility within ±3000 bp of
442 annotated TSS (Figure 4D). Surprisingly, cell depolarization had little effect on global chromatin
443 alterations associated with these three CTPs, with 72.7%, 85%, 79.1 % and of ATAC-seq peaks
444 overlapping in resting versus depolarized cells, for α1CCT, α1ACT, and α1HCT, respectively
445 (Figure 4E). Furthermore, approximately 238 of ATAC-seq peaks overlap among these three
446 CTPs in resting cells, and 222 in the presence of 20mM KCl (Figure 4F), suggesting that the

447 CTPs have overlapping effects on global transcriptional alterations, despite their distinct gene
448 binding profiles induced by cell depolarization.

449

450 **α1CCT, α1ACT, and α1HCT mediate a neurodevelopmental program in a calcium-**
451 **dependent manner in hNPCs**

452 To explore the functional pathways regulated by α1CCT, α1ACT, or α1HCT through chromatin
453 modulation or binding, we conducted RNA-seq analyses on stable hNPC cell lines expressing
454 α1CCT, α1ACT, or α1HCT, at DIV5, and compared them with the empty pLVX vector in
455 resting conditions only. Using RNA-seq, we identified 1007, 2949, and 3192 differentially
456 expressed genes (DEGs) in α1CCT-, α1ACT-, or α1HCT- overexpressing hNPCs, respectively
457 (Figure 5A). Integration of the CUT&RUN-seq and RNA-seq analyses revealed that 13.4%,
458 29%, or 9.24% of RNA-seq DEGs were correlated with direct DNA binding for α1CCT, α1ACT,
459 or α1HCT (C&R-DEGs), respectively (Figure S5A). Therefore, α1CCT, α1ACT, or α1HCT, as
460 independent DNA binding proteins, target specific genes and directly regulate their expression.
461 To correlate these results with those assessing chromatin accessibility, we integrated the ATAC-
462 seq and RNA-seq analyses, which showed that 51.9%, 65.7%, or 66% of RNA-seq DEGs
463 overlapped with ATAC-seq peaks (ATAC-DEGs) for α1CCT, α1ACT, or α1HCT, respectively
464 (Figure S5B). These findings demonstrate that the three VGCC CTPs alter the transcriptional
465 profile in hNPCs by modulating chromatin accessibility.

466 We performed Gene Ontology (GO) term analysis on RNA-seq integrated genes that
467 were also identified by ATAC-seq or CUT&RUN-seq. For α1CCT, ATAC-DEGs showed
468 enrichment in pathways related to synaptic transmission, axonogenesis, and transmembrane

469 transport under both conditions (Figure S5C). However, α1CCT-associated C&R-DEGs were
470 specifically linked to ion transmembrane transport and developmental growth, with these
471 associations observed only under cell depolarizing conditions (Figure 5B). For α1ACT, ATAC-
472 DEGs and C&R-DEGs were associated with neurogenesis, embryonic organ development, and
473 synapse formation, in both high and low KCl conditions (Figure S5D). However, in the cell-
474 depolarized condition, more neurogenesis-related genes and pathways were annotated among the
475 DEG-C&R genes (Figure 5C). The results indicate that α1ACT regulates a set of neurogenesis
476 genes basally but activates a larger ensemble for neurogenesis during neuronal activity. The top-
477 ranked α1HCT ATAC-DEGs were associated with axon development, neuronal projection,
478 development and guidance, and cell migration in both conditions (Figure S5E). For the α1HCT-
479 associated C&R-DEGs, neuron-related pathways, including axon development, neuron
480 migration, and synapse organization, were identified exclusively under cell-depolarized
481 conditions (Figure 5D).

482 These results revealed that, among the DNA binding-regulated DEGs for α1CCT,
483 α1ACT, and α1HCT, GO terms related to neuronal growth/neurogenesis, synapse formation, and
484 ion channels are enriched, and overlapped. More interestingly, for α1CCT, α1ACT and α1HCT,
485 neuronal growth-related pathways were predominantly enriched in C&R-DEGs in depolarized
486 cells, a pattern not observed in ATAC-DEGs. These findings indicate that the transcriptional
487 regulation of neuronal growth pathways associated with the three VGCC CTPs is enhanced by
488 VGCC-induced Ca^{2+} signaling.

489

490 **α1CCT, α1ACT, and α1HCT have distinct calcium-responsive regulatory profiles in**
491 **hNPCs**

492 To further dissect the regulatory mechanisms underlying these transcriptional changes, we
493 performed TF motif enrichment analysis using C&R-DEGs, which uncovered unique TF binding
494 profiles for α1CCT, α1ACT, and α1HCT in hNPCs under basal and depolarized conditions.
495 α1CCT exhibited a binding profile enriched in motifs for homeobox (HOXA1) and HMG (Sox7)
496 TFs in basal conditions, while in depolarized states, it was associated with motifs for homeobox
497 factors (Six4, Lhx1) (Figure 5E). α1ACT bound to motifs for bZIP (JunB), and STAT (STAT4)
498 families in basal conditions, whereas in depolarized conditions, it recognized motif for bZIP(c-
499 Jun-CRE) and ATAA/TATT (GATA 1.2.3.4) factors (Figure 5F). α1HCT had a binding profile
500 enriched for nuclear receptor (NR) motifs (ERRα, Nr5a2) in basal conditions, while in
501 depolarized states, it recognized Homeobox (Six2) and Zf (HINFP) motifs (Figure 5G). These
502 motif binding profiles suggest that α1CCT, α1ACT, and α1HCT engage in different neuronal
503 activity-related regulatory programs, underscoring their potential roles in neural differentiation
504 and development. While their motif preferences are distinct, their biological functions appear to
505 overlap.

506 Our findings indicate that the distinct transcriptional regulation mediated by α1CCT,
507 α1ACT, and α1HCT is driven by their ability to interact with specific TF motifs, dynamically
508 responding to KCl-induced depolarization. This coordination links their chromatin-modifying
509 functions to transcription factor-driven gene expression changes, highlighting their role as Ca^{2+}-
510 dependent regulators of transcription in hNPCs.

511

512 **Verified DEGs for α1CCT, α1ACT, and α1HCT in neuronal expression and synaptic**
513 **regulation**

514 Following the identification of DEGs for α1CCT, α1ACT, and α1HCT through next-generation
515 sequencing, we validated key targets using TaqMan qRT-PCR assays, focusing on genes that
516 overlapped with CUT&RUN (C&R) and ATAC-seq data. The validated α1CCT target genes,
517 including *KCNQ2*, *MAPT*, and *NPAS3*, are strongly associated with neuronal excitability and ion
518 translation. Additionally, we verified ATAC-seq confirmed genes such as *PTN*, *MAPK10*,
519 *GABRA5*, *CAMK2B*, and *CPLX2*, reinforcing the involvement of α1CCT in synaptic plasticity,
520 neurotransmission, and Ca^{2+}-dependent signaling (Figure S5F). α1ACT directly regulates genes
521 such as *FGFR2*, *SYNDIG1*, *NCAM2*, *GABRG1*, and *NLGN*, indicating roles in neurogenesis,
522 synapse formation, and synaptic adhesion (Figure S5G). Verification of ATAC-DEGs—*ASTN2*,
523 *MDGA1*, *VSNL1*, *SPON1*, *WNT2*, *RYR2*, *SHANK2*, and *PTGER3*— suggests that α1ACT has
524 additional functions in neuronal migration, Wnt signaling, and excitatory synapse maturation
525 (Figure S5G). For α1HCT, validated genes, such as *PTPRD*, suggest roles in neuronal
526 connectivity and synapse organization, while the ATAC-seq-confirmed targets *SEMA3A* and
527 *MEF2C* highlight its function in axon guidance, neuronal migration, and synaptic remodeling
528 (Figure S5H). This suggests that α1HCT preferentially regulates axon development and neural
529 circuit formation. These validated genes highlight that each VGCC CTP regulates distinct, yet
530 overlapping, transcriptional programs, contributing to neuronal differentiation, synaptic
531 organization, and neurodevelopmental signaling pathways.

532

533 **α1CCT, α1ACT, and α1HCT induce a neuronal phenotype in hNPCs**

534 The transcriptional changes induced by α1CCT, α1ACT, and α1HCT suggest a broader impact
535 on neuronal differentiation and morphology. Consistent with these findings, we observed that
536 many of the validated DEGs are linked to neurite outgrowth, synaptic development, and

537 cytoskeletal dynamics, raising the possibility that these VGCC CTPs may promote structural
538 changes in hNPCs. While conducting genomic and transcriptomic studies on hNPCs stably
539 expressing CTPs, we observed notable changes in cellular phenotype, with increases in neurite
540 morphologies. We found that hNPCs expressing any one of the three CTPs grew significantly
541 more neurites than the empty vector control stable line at DIV5 (α1CCT: 2.90±0.22 neurites;
542 α1ACT: 2.75±0.23 neurites; α1HCT: 3.63±0.25 neurites vs control: 1.53±0.16 neurites, $p <$
543 0.002) (Figure 6A-B). Additionally, hNPCs expressing α1CCT, α1ACT and α1HCT significantly
544 increased the "longest neurite length" compared to the control stable line (α1CCT: 90.75±10.60
545 μm; α1ACT: 66.55±7.68 μm; α1HCT: 74.62±9.16 μm, $p < 0.001$vs control: 32.44±5.46 μm) and
546 the average neurite length (Figure 6C and D).

547 Taken together, these findings indicate that the novel VGCC CTPs, α1CCT, α1ACT, and
548 α1HCT mediate widespread changes in gene expression, promoting the development or
549 maturation of a neuronal phenotype.

550

551 **α1CCT restores disrupted gene expression in a forebrain-specific *CACNA1C* knockout**
552 **mouse**

553 We previously demonstrated that transgenic expression of α1ACT in *CACNA1A*-deficient mice
554 improves survival and ataxic behavior, and restores expression of α1ACT-regulated genes (Du et
555 al., 2019). L-type VGCCs, and most notably $Ca_v1.2$ (encoded by *Cacna1c*), play a critical role
556 in both cardiac and neuronal function, as well as activity Ca^{2+}-dependent transcriptional
557 regulation (Dolmetsch et al., 2001; Kandel, 2001; Li et al., 2016a; Raymond, 2007; Wheeler et
558 al., 2008; Wheeler et al., 2012; Wu et al., 2001). As a test case to relate CTP-regulated gene

559 expression to the parent VGCC gene *in vivo*, we used AAV9-mediated delivery of α1CCT in a
560 conditional forebrain knockout mouse model (Forebrain-*Cacna1c* cKO), as complete *Cacna1c*
561 knockouts are non-viable. In this mouse model, a floxed *Cacna1c* allele is deleted selectively in
562 forebrain neurons expressing Cre under a CaMKII transgene promoter (Figure 6E and S6A) (Lee
563 et al., 2012).

564 To selectively express α1CCT in Cre-expressing, *Cacna1c*-null neurons, we employed
565 AAV9 vectors that use a Double Flox Inverted Open Read Frame (DIO) system, enabling
566 conditional expression of α1CCT protein in forebrain neurons. Forebrain-*Cacna1c* cKO mice
567 (P0-P1) were injected via the lateral ventricles with AAV virus expressing either control EmGFP
568 (AAV9-FLEX-EmGFP) or α1CCT (AAV9-FLEX- α1CCT:P2A:EmGFP) (Figure 6E and G). At
569 P30-35, forebrain tissue was sectioned for laser capture microdissection (LCM) to isolate
570 EmGFP-labeled cortical neurons for TaqMan qRT-PCR analysis (Figure 6F and G).

571 Expression analysis revealed significant downregulation of α1CCT-regulated DEGs, such
572 as *Npas3* (-11.54±7.7%), *Kcnq2* (-24.79±12.0%), *Snap25* (-36.41±8.8%), *Grm1*(-32.03±10.0%),
573 and *Htr3a* (-76.1±17.1%) in the Forebrain-*Cacna1c* cKO mice receiving AAV-EmGFP virus,
574 compared to wild-type mice receiving AAV-EmGFP virus (Figure 6G). More importantly, the
575 expression of these genes was rescued to normal or significantly higher levels in cells expressing
576 α1CCT (*Npas3:* 47.64±12.0%; *Snap25:* 51.7±6.7%; *Grm1*(41.13±13.6%), *Htr3a:*
577 106.43±30.7%) (Figure 6G).

578 These results show that lack of *Cacna1c* impacts the gene expression profile of α1CCT in
579 cortical neurons, but *in vivo* re-expression of α1CCT alone rescues the expression of both
580 α1CCT-regulated DEGs and chromatin accessibility DEGs. These rescued genes are involved in
581 synaptic transmission (*Snap25*), ion transport (*Kcnq2*), neurogenesis (*Npa3*), and

582 neurotransmitter receptors (*Grm1*and *Htr3a*). Taken together, these findings indicate that
583 α1CCT, as an independent protein, plays an important role in promoting maturation of a
584 neuronal phenotype.

585

586 **Discussion:**

587 This study provides evidence for the presence of a conserved genetic strategy across the entire
588 VGCC gene family that enables direct signaling to the nucleus by a set of C-terminal
589 transcription factors coupled to, and co-expressed with, the VGCC channel proteins. The co-
590 expressed C-terminal proteins are encoded by overlapping cistrons in the same mRNA.
591 Translation of the 70-75kD CTPs, α1CCT, α1ACT, and α1HCT, occurs by means of IRES-like
592 structures within the α1C, α1A, and α1H mRNAs. In addition to the *genetic* coupling of the
593 channel protein to the co-expressed transcription factor, we have identified *physiological*
594 coupling of ion channel activity to the behavior of the same transcription factor. We find that the
595 nuclear translocation of α1CCT and α1ACT is influenced by cellular Ca^{2+} currents in neurons in
596 real-time. Moreover, cell-depolarizing conditions dramatically alter the gene binding profiles of
597 α1CCT, α1ACT and α1HCT, indicating a *direct link* between Ca^{2+}-dependent VGCC activity
598 and transcriptional regulation. These Ca^{2+} currents facilitate the nuclear-cytoplasmic
599 translocation of VGCC CTPs, which in turn directly activates ensembles of DEGs that are
600 crucial for the development of neuronal phenotypes, particularly neurogenesis, synaptic
601 formation, and ion channel transport, in concert with the emergence of neuronal activity.
602 Ultimately, the transcriptional functions of α1CCT, α1ACT and α1HCT are highly integrated
603 with Ca^{2+}-induced nuclear signaling, shaping neuronal connectivity and synaptic function.

604

605 Co-expression of membrane receptors and nuclear signaling molecules has been
606 typically associated with a protease cleavage event that liberates the signaling molecule, as in the
607 cases of amyloid precursor protein, Notch receptor, and ERBB2/Her2, although the capacity for
608 IRES-based expression has also been reported in some isoforms of Notch receptor and
609 ERBB2/Her2 (Godfrey et al., 2022; Karginov et al., 2017; Lauring and Overbaugh, 2000). While
610 our findings do not exclude the existence of other cellular pathways for generating Ca^{2+} channel
611 CTPs, such as protease cleavage and cryptic promoters (Gomez-Ospina et al., 2013; Hulme et
612 al., 2006), this study demonstrates the pervasive expression of CTPs broadly within the VGCC
613 gene family by an internal translation process. Of these, we formally confirmed that α1CCT,
614 α1ACT, and α1HCT, representing the three subfamilies of VGCC genes, are translated by a cap-
615 independent translation mechanism. Moreover, this expression strategy of CTPs appears to be
616 accompanied by nuclear signaling, as we identified CTPs expressed by all ten VGCC genes
617 translocating to the nucleus.

618

619 Key domains within the Ca^{2+} channel C-termini have been identified as mediators of Ca^{2+}
620 channel function, specifically those that competitively modulate Ca^{2+} channel gating processes
621 by inhibiting Ca^{2+}-dependent inactivation (CDI) (Bock et al., 2011; Castiglioni et al., 2006; Liu
622 et al., 2017; Singh et al., 2006; Wahl-Schott et al., 2006), or that bind synaptic vesicles to initiate
623 their delivery to the active zone (Gardezi et al., 2016; Wong et al., 2014). In some of these
624 studies, the capacity for modulation of full-length Ca^{2+} channel function via the C-terminus was
625 noted even when C-terminal fragments were co-expressed with full-length channels. Thus, we
626 cannot exclude an additional role for cytoplasmic CTPs in potentially modulating Ca^{2+} currents

627 to influence their nuclear translocation. As shown here, all ten VGCC CTPs distribute between
628 the cytoplasm and nucleus, albeit at different rates, and translocation of α1CCT and α1ACT was
629 driven by Ca^{2+} influx through specific channels. Interestingly, none of the brief stimuli used in
630 this study had a significant effect on the subcellular localization of α1HCT, even though there
631 was a trend towards increasing nuclear Ca^{2+} fluorescence in live primary rat cortical neurons. It
632 is possible that the localization and translocation of the *CACNA1H*-derived CTP may be
633 independent of Ca^{2+}signaling over the short time course used here, or through other processes.

634

635 Ca^{2+} is a ubiquitous cellular second messenger that plays a vital role in almost every facet
636 of neuronal development, maturation, and maintenance, by signaling to TFs, such as NFAT and
637 CREB (Hardingham et al., 2001; Li et al., 2016b; Wheeler et al., 2012). VGCC channels link
638 Ca^{2+} entry through electrical activity to nuclear gene expression. VGCCs serve as key Ca^{2+}
639 signal transducers, and Ca^{2+} influx through them mediates a wide variety of downstream
640 physiological events (Berridge, 2014). Previously, Gomez-Ospina et al. showed that the CTP of
641 $Ca_V1.2$ (α1CCT) acts as an independent TF that regulates a group of neuronal genes, and that its
642 translocation is influenced by Ca^{2+}, although they did not elucidate the relationship between Ca^{2+}
643 signaling and gene regulation. Yang et al. reported the role of cytosolic and nuclear DCT of
644 $Ca_V1.3$ (α1DCT) in regulating neurogenesis and channel activity. Our group previously
645 demonstrated that α1ACT is a critial TF in cerebellar development (Du et al., 2013; Du et al.,
646 2019; Gomez-Ospina et al., 2006; Yang et al., 2022). This study extends the findings of
647 previous Ca^{2+} channel studies and paints a global picture of Ca^{2+} channel direct signaling to the
648 nucleus, by establishing an additional connection between Ca^{2+} and the secondary CTP gene
649 products of the VGCC genes.

650

651 In this study, we utilized the CUT & RUN-seq technique, coupled with ATAC-seq and
652 RNA-seq, to analyze the genomic and transcriptomic profiles of α1CCT, α1ACT, and α1HCT
653 expressed in hNPCs. Our findings reveal that, for all three CTPs, Ca^{2+} influx plays a critical role
654 in mediating their biological function. On the one hand, 222 (resting)/238 (depolarized) genes
655 that show altered chromatin accessibility have been identified in common among three CTP-
656 overexpressing hNPCs. Interestingly, the majority of these gene appear to function in promoting
657 neuronal growth pathways and are not influenced by Ca^{2+} influx. On the other hand, each CTP is
658 associated with distinct TF motifs, without overlap among all three, and this could contribute to
659 the regulation of specific genes for neurodevelopment, synaptic formation, and ion membrane
660 transport in response to Ca^{2+} influx. For instance, an AT-rich motif was previously identified for
661 α1ACT (Du et al., 2013). Meanwhile, there was a 20 - 30% overlap between DEGs in hNPCs
662 and those associated with neurite outgrowth, with 10 of these genes verified in α1ACT-
663 expressing transgenic mice and rescued by α1ACT (Du et al., 2019). These findings reinforce the
664 established role of Ca^{2+} as a second messenger, by demonstrating that the three co-expressed
665 VGCC proteins, α1CCT, α1ACT and α1HCT, drive expression of neuronal genes. These CTPs
666 act in concert with the emergence of neuronal activity, enhancing Ca^{2+} efficiency as a mediator
667 of nuclear-cytoplasmic translocation and gene regulation.

668

669 While the genetic organization observed for the Ca^{2+} channel and its CTPs appears to
670 facilitate efficient coordination of gene activation, it also increases the likelihood that genetic
671 disruptions will have intricate downstream consequences and may help explain some of the
672 complex clinical phenotypes seen with VGCC gene mutations. Loss- or gain-of-function

673 mutations in the *CACNA1C* gene, encoding the α1C ($Ca_v1.2$) L-type Ca^{2+} channel subunit, are
674 associated with a pleiotropic set of disorders including the autism spectrum disorder (ASD)
675 Timothy Syndrome, bipolar disorder, schizophrenia, and major depressive disorder (MDD), as
676 well as severe cardiac defects (Boczek et al., 2013; Boczek et al., 2015; Cross-Disorder Group of
677 the Psychiatric Genomics, 2013; Dedic et al., 2018; Green et al., 2010; Splawski et al., 2004).
678 Loss- or gain-of-function mutations in the *CACNA1A* gene, encoding the α1A ($Ca_v2.1$) P/Q-type
679 Ca^{2+} channel subunit, may lead to ataxia, hemiplegic migraine, epilepsy, or cognitive disability
680 (Indelicato et al., 2018). Mutations in the α1H ($Ca_v3.2$) subunit, part of the T-type VGCC, are
681 associated with chronic neuropathic pain disorders, ASD, and several types of mental illness
682 (Becker et al., 2017; Carter et al., 2019; Heron et al., 2007; Lee et al., 2018; Rzhepetskyy et al.,
683 2016; Souza et al., 2016; Splawski et al., 2006; Stringer et al., 2020). Given that such mutations
684 across the coding regions of these genes may have a positive or negative effect on the function of
685 a channel, the co-expressed transcription factor, or the regulation or translocation of that
686 transcription factor, this diversity of phenotypes may arise from a disruption of the complex
687 dynamics of these two-protein/one-gene systems. Unsurprisingly, attempts to recapitulate such
688 phenotypically complex disorders in animal models have often fallen short of providing an
689 understanding of pathogenesis.

690

691 In conclusion, this study identifies a pervasive dual protein expression system within the
692 VGCC gene family and sheds new light on the intricate genetic and physiological coordination
693 inherent in members of the VGCC gene family. Our findings establish a direct link between
694 Ca^{2+} channel activity and nuclear gene expression through the co-expression and translocation of
695 CTPs. This dual-protein mechanism underscores the importance of Ca^{2+} as a critical second

696 messenger that extends its influence from the cellular membrane, where Ca^{2+} channels reside, to
697 the nuclear CTPs, thereby orchestrating complex gene regulatory networks essential for
698 neurogenesis, synaptic formation, and ion channel transport. This coordinated process adds to the
699 previously identified TFs a new set of gene regulatory proteins, the *calcium channel-coupled*
700 *transcription factors*, as CTPs co-expressed with the VGCC channel proteins. The operation of
701 this dual-protein system as a self-regulatory mechanism under physiological conditions will
702 require further study. Additionally, since mutations in these genes result in multifaceted clinical
703 phenotypes, this study provides valuable insights into the mechanisms that underlie neuronal
704 phenotypes and their potential perturbations in disease states, paving the way for novel
705 therapeutic strategies to target the VGCC gene family, such as modulating channel function,
706 RNA silencing, or viral delivery of CTP transcription factors.

707

708 **Statistical analysis**

709 Statistical analyses were conducted using GraphPad Prism 7 software (GraphPad Software Inc.,
710 La Jolla, CA), RStudio (Boston, MA), and SPSS (IBM, Armonk, NY). For single comparisons,
711 Student's t test was used to establish statistical significance. For multiple sample comparisons,
712 One-Way ANOVA was performed, followed by Student-Newman-Keuls Method post hoc tests.
713 Data were expressed as the mean ± SEM and written with the identification of n under
714 appropriate figure legends, with $*p < 0.05$, $**p < 0.01$; $***p < 0.001$.

715

716 **Data and Code availability**

717 All data reported in this paper will be publicly available upon manuscript publication in an
718 online database or via request to the corresponding authors. All source code will be deposited at
719 Github. Further additional information and requests should be addressed to lead contact,
720 Christopher M. Gomez (gomez001@uchicago.edu)

721

722 **Acknowledgments**

723 This work was supported by NIH grants: R01NS082788, R01NS094665, R35NS116868
724 (C.M.G.), a Floyd family donation, and Margaret Hackett Family Program Translational
725 Research Award. We thank Dr. Sally Rowland and Dr. Xiaoxi Zhuang for comments on the
726 manuscript; Drs. Vytas Bindokas and Christine Labno at the University of Chicago Microscopy
727 Core Facility for the imaging service.

728

729 **Author Contributions**

730 E.R., X.D. and C.M.G. conceived the project. E.R., X.D. and C.M.G. designed the study and
731 experiments. E.R., T.T., J.G., D.H., and E.G., performed the most experiments, Q.L. Y.L. and
732 C.W. analyzed the ChIP and RNA-seq data. C.W. was in charge of mice breeding and phenotyping.
733 E.R., T.T., X.D., and C.M.G. wrote the manuscript with input from all coauthors.

734 **Author Declaration of Interests**

735 The authors declare no competing interests.

736 **References**

737 Adams, M.E., Bindokas, V.P., Hasegawa, L., and Venema, V.J. (1990). Omega-agatoxins: novel calcium
738 channel antagonists of two subtypes from funnel web spider (Agelenopsis aperta) venom. J Biol Chem
739 *265*, 861-867.
740 Andrade, A., Sandoval, A., Oviedo, N., De Waard, M., Elias, D., and Felix, R. (2007). Proteolytic cleavage
741 of the voltage-gated Ca2+ channel alpha2delta subunit: structural and functional features. Eur J
742 Neurosci *25*, 1705-1710.
743 Bannister, J.P., Leo, M.D., Narayanan, D., Jangsangthong, W., Nair, A., Evanson, K.W., Pachuau, J.,
744 Gabrick, K.S., Boop, F.A., and Jaggar, J.H. (2013). The voltage-dependent L-type Ca2+ (CaV1.2) channel C-
745 terminus fragment is a bi-modal vasodilator. J Physiol *591*, 2987-2998.
746 Beals, C.R., Sheridan, C.M., Turck, C.W., Gardner, P., and Crabtree, G.R. (1997). Nuclear export of NF-ATc
747 enhanced by glycogen synthase kinase-3. Science *275*, 1930-1934.
748 Becker, F., Reid, C.A., Hallmann, K., Tae, H.S., Phillips, A.M., Teodorescu, G., Weber, Y.G., Kleefuss-Lie, A.,
749 Elger, C., Perez-Reyes, E*., et al.* (2017). Functional variants in HCN4 and CACNA1H may contribute to
750 genetic generalized epilepsy. Epilepsia Open *2*, 334-342.
751 Belfield, J.L., Whittaker, C., Cader, M.Z., and Chawla, S. (2006). Differential effects of Ca2+ and cAMP on
752 transcription mediated by MEF2D and cAMP-response element-binding protein in hippocampal neurons.
753 J Biol Chem *281*, 27724-27732.
754 Berridge, M.J. (2014). Calcium signalling and psychiatric disease: bipolar disorder and schizophrenia. Cell
755 Tissue Res *357*, 477-492.
756 Best, J.M., and Kamp, T.J. (2012). Different subcellular populations of L-type Ca2+ channels exhibit
757 unique regulation and functional roles in cardiomyocytes. J Mol Cell Cardiol *52*, 376-387.
758 Bock, G., Gebhart, M., Scharinger, A., Jangsangthong, W., Busquet, P., Poggiani, C., Sartori, S., Mangoni,
759 M.E., Sinnegger-Brauns, M.J., Herzig, S*., et al.* (2011). Functional properties of a newly identified C-
760 terminal splice variant of Cav1.3 L-type Ca2+ channels. J Biol Chem *286*, 42736-42748.
761 Boczek, N.J., Best, J.M., Tester, D.J., Giudicessi, J.R., Middha, S., Evans, J.M., Kamp, T.J., and Ackerman,
762 M.J. (2013). Exome sequencing and systems biology converge to identify novel mutations in the L-type
763 calcium channel, CACNA1C, linked to autosomal dominant long QT syndrome. Circ Cardiovasc Genet *6*,
764 279-289.
765 Boczek, N.J., Ye, D., Jin, F., Tester, D.J., Huseby, A., Bos, J.M., Johnson, A.J., Kanter, R., and Ackerman,
766 M.J. (2015). Identification and Functional Characterization of a Novel CACNA1C-Mediated Cardiac
767 Disorder Characterized by Prolonged QT Intervals With Hypertrophic Cardiomyopathy, Congenital Heart
768 Defects, and Sudden Cardiac Death. Circ Arrhythm Electrophysiol *8*, 1122-1132.
769 Bortone, D., and Polleux, F. (2009). KCC2 expression promotes the termination of cortical interneuron
770 migration in a voltage-sensitive calcium-dependent manner. Neuron *62*, 53-71.
771 Carter, M.T., McMillan, H.J., Tomin, A., and Weiss, N. (2019). Compound heterozygous CACNA1H
772 mutations associated with severe congenital amyotrophy. Channels (Austin) *13*, 153-161.
773 Castiglioni, A.J., Raingo, J., and Lipscombe, D. (2006). Alternative splicing in the C-terminus of CaV2.2
774 controls expression and gating of N-type calcium channels. J Physiol *576*, 119-134.
775 Chemin, J., Taiakina, V., Monteil, A., Piazza, M., Guan, W., Stephens, R.F., Kitmitto, A., Pang, Z.P.,
776 Dolphin, A.C., Perez-Reyes, E*., et al.* (2017). Calmodulin regulates Ca(v)3 T-type channels at their gating
777 brake. J Biol Chem *292*, 20010-20031.
778 Cipriano, L., Piscopo, R., Aiello, C., Novelli, A., Iolascon, A., and Piscopo, C. (2024). Expanding the
779 Phenotype of the CACNA1C-Associated Neurological Disorders in Children: Systematic Literature Review
780 and Description of a Novel Mutation. Children (Basel) *11*.
781 Cross-Disorder Group of the Psychiatric Genomics, C. (2013). Identification of risk loci with shared
782 effects on five major psychiatric disorders: a genome-wide analysis. Lancet *381*, 1371-1379.
783 Darcy, D.P., and Isaacson, J.S. (2009). L-type calcium channels govern calcium signaling in migrating
784 newborn neurons in the postnatal olfactory bulb. J Neurosci *29*, 2510-2518.

785 Dedic, N., Pohlmann, M.L., Richter, J.S., Mehta, D., Czamara, D., Metzger, M.W., Dine, J., Bedenk, B.T.,
786 Hartmann, J., Wagner, K.V.*, et al.* (2018). Cross-disorder risk gene CACNA1C differentially modulates
787 susceptibility to psychiatric disorders during development and adulthood. Mol Psychiatry *23*, 533-543.
788 Deisseroth, K., Heist, E.K., and Tsien, R.W. (1998). Translocation of calmodulin to the nucleus supports
789 CREB phosphorylation in hippocampal neurons. Nature *392*, 198-202.
790 Dolmetsch, R.E., Pajvani, U., Fife, K., Spotts, J.M., and Greenberg, M.E. (2001). Signaling to the nucleus
791 by an L-type calcium channel-calmodulin complex through the MAP kinase pathway. Science *294*, 333-
792 339.
793 Du, X., Wang, J., Zhu, H., Rinaldo, L., Lamar, K.M., Palmenberg, A.C., Hansel, C., and Gomez, C.M. (2013).
794 Second cistron in CACNA1A gene encodes a transcription factor mediating cerebellar development and
795 SCA6. Cell *154*, 118-133.
796 Du, X., Wei, C., Hejazi Pastor, D.P., Rao, E.R., Li, Y., Grasselli, G., Godfrey, J., Palmenberg, A.C., Andrade,
797 J., Hansel, C.*, et al.* (2019). alpha1ACT Is Essential for Survival and Early Cerebellar Programming in a
798 Critical Neonatal Window. Neuron *102*, 770-785 e777.
799 Follesa, P., and Ticku, M.K. (1996). NMDA receptor upregulation: molecular studies in cultured mouse
800 cortical neurons after chronic antagonist exposure. J Neurosci *16*, 2172-2178.
801 Gardezi, S.R., Nath, A.R., Li, Q., and Stanley, E.F. (2016). Characterization of a Synaptic Vesicle Binding
802 Motif on the Distal CaV2.2 Channel C-terminal. Front Cell Neurosci *10*, 145.
803 Ge, J., Ju, Y., Xue, Z., Feng, Y., Huang, X., Liu, H., and Zhao, S. (2013). Distal C terminus of CaV1.2 channels
804 plays a crucial role in the neural differentiation of dental pulp stem cells. PLoS One *8*, e81332.
805 Godfrey, J.D., Hejazi, D., Du, X., Wei, C., Rao, E., and Gomez, C.M. (2022). HER2 c-Terminal Fragments
806 Are Expressed via Internal Translation of the HER2 mRNA. Int J Mol Sci *23*.
807 Goldstein, I., and Hager, G.L. (2018). Dynamic enhancer function in the chromatin context. Wiley
808 Interdiscip Rev Syst Biol Med *10*.
809 Gomez-Ospina, N., Panagiotakos, G., Portmann, T., Pasca, S.P., Rabah, D., Budzillo, A., Kinet, J.P., and
810 Dolmetsch, R.E. (2013). A Promoter in the Coding Region of the Calcium Channel Gene CACNA1C
811 Generates the Transcription Factor CCAT. PLoS One *8*, e60526.
812 Gomez-Ospina, N., Tsuruta, F., Barreto-Chang, O., Hu, L., and Dolmetsch, R. (2006). The C terminus of
813 the L-type voltage-gated calcium channel Ca(V)1.2 encodes a transcription factor. Cell *127*, 591-606.
814 Govindaraj, K., Hendriks, J., Lidke, D.S., Karperien, M., and Post, J.N. (2019). Changes in Fluorescence
815 Recovery After Photobleaching (FRAP) as an indicator of SOX9 transcription factor activity. Biochim
816 Biophys Acta Gene Regul Mech *1862*, 107-117.
817 Green, E.K., Grozeva, D., Jones, I., Jones, L., Kirov, G., Caesar, S., Gordon-Smith, K., Fraser, C., Forty, L.,
818 Russell, E.*, et al.* (2010). The bipolar disorder risk allele at CACNA1C also confers risk of recurrent major
819 depression and of schizophrenia. Mol Psychiatry *15*, 1016-1022.
820 Hagenston, A.M., Rudnick, N.D., Boone, C.E., and Yeckel, M.F. (2009). 2-Aminoethoxydiphenyl-borate (2-
821 APB) increases excitability in pyramidal neurons. Cell Calcium *45*, 310-317.
822 Hardingham, G.E., Arnold, F.J., and Bading, H. (2001). Nuclear calcium signaling controls CREB-mediated
823 gene expression triggered by synaptic activity. Nat Neurosci *4*, 261-267.
824 Heron, S.E., Khosravani, H., Varela, D., Bladen, C., Williams, T.C., Newman, M.R., Scheffer, I.E., Berkovic,
825 S.F., Mulley, J.C., and Zamponi, G.W. (2007). Extended spectrum of idiopathic generalized epilepsies
826 associated with CACNA1H functional variants. Ann Neurol *62*, 560-568.
827 Hulme, J.T., Yarov-Yarovoy, V., Lin, T.W., Scheuer, T., and Catterall, W.A. (2006). Autoinhibitory control
828 of the CaV1.2 channel by its proteolytically processed distal C-terminal domain. J Physiol *576*, 87-102.
829 Kandel, E.R. (2001). The molecular biology of memory storage: a dialogue between genes and synapses.
830 Science *294*, 1030-1038.
831 Karginov, T.A., Pastor, D.P.H., Semler, B.L., and Gomez, C.M. (2017). Mammalian Polycistronic mRNAs
832 and Disease. Trends Genet *33*, 129-142.

833 Komuro, H., and Rakic, P. (1996). Intracellular Ca2+ fluctuations modulate the rate of neuronal
834 migration. Neuron *17*, 275-285.
835 Kordasiewicz, H.B., Thompson, R.M., Clark, H.B., and Gomez, C.M. (2006). C-termini of P/Q-type Ca2+
836 channel alpha1A subunits translocate to nuclei and promote polyglutamine-mediated toxicity. Hum Mol
837 Genet *15*, 1587-1599.
838 Kraus, R.L., Li, Y., Gregan, Y., Gotter, A.L., Uebele, V.N., Fox, S.V., Doran, S.M., Barrow, J.C., Yang, Z.Q.,
839 Reger, T.S.*, et al.* (2010). In vitro characterization of T-type calcium channel antagonist TTA-A2 and in
840 vivo effects on arousal in mice. J Pharmacol Exp Ther *335*, 409-417.
841 Lauring, A.S., and Overbaugh, J. (2000). Evidence that an IRES within the Notch2 coding region can direct
842 expression of a nuclear form of the protein. Mol Cell *6*, 939-945.
843 Leake, M.C. (2018). Transcription factors in eukaryotic cells can functionally regulate gene expression by
844 acting in oligomeric assemblies formed from an intrinsically disordered protein phase transition enabled
845 by molecular crowding. Transcription *9*, 298-306.
846 Lee, A.S., Ra, S., Rajadhyaksha, A.M., Britt, J.K., De Jesus-Cortes, H., Gonzales, K.L., Lee, A., Moosmang,
847 S., Hofmann, F., Pieper, A.A.*, et al.* (2012). Forebrain elimination of cacna1c mediates anxiety-like
848 behavior in mice. Mol Psychiatry *17*, 1054-1055.
849 Lee, C.G., Lee, J., and Lee, M. (2018). Multi-gene panel testing in Korean patients with common genetic
850 generalized epilepsy syndromes. PLoS One *13*, e0199321.
851 Li, B., Tadross, M.R., and Tsien, R.W. (2016a). Sequential ionic and conformational signaling by calcium
852 channels drives neuronal gene expression. Science *351*, 863-867.
853 Li, W., Zheng, N.Z., Yuan, Q., Xu, K., Yang, F., Gu, L., Zheng, G.Y., Luo, G.J., Fan, C., Ji, G.J.*, et al.* (2016b).
854 NFAT5-mediated CACNA1C expression is critical for cardiac electrophysiological development and
855 maturation. J Mol Med (Berl) *94*, 993-1002.
856 Linseman, D.A., Bartley, C.M., Le, S.S., Laessig, T.A., Bouchard, R.J., Meintzer, M.K., Li, M., and
857 Heidenreich, K.A. (2003). Inactivation of the myocyte enhancer factor-2 repressor histone deacetylase-5
858 by endogenous Ca(2+) //calmodulin-dependent kinase II promotes depolarization-mediated cerebellar
859 granule neuron survival. J Biol Chem *278*, 41472-41481.
860 Liu, N., Yang, Y., Ge, L., Liu, M., Colecraft, H.M., and Liu, X. (2017). Cooperative and acute inhibition by
861 multiple C-terminal motifs of L-type Ca(2+) channels. Elife *6*.
862 Mao, Z., Bonni, A., Xia, F., Nadal-Vicens, M., and Greenberg, M.E. (1999). Neuronal activity-dependent
863 cell survival mediated by transcription factor MEF2. Science *286*, 785-790.
864 Mattson, M.P., Lovell, M.A., Ehmann, W.D., and Markesbery, W.R. (1993). Comparison of the effects of
865 elevated intracellular aluminum and calcium levels on neuronal survival and tau immunoreactivity. Brain
866 Res *602*, 21-31.
867 Mattson, M.P., Rychlik, B., Chu, C., and Christakos, S. (1991). Evidence for calcium-reducing and excito-
868 protective roles for the calcium-binding protein calbindin-D28k in cultured hippocampal neurons.
869 Neuron *6*, 41-51.
870 Miyazaki, Y., Du, X., Muramatsu, S., and Gomez, C.M. (2016). An miRNA-mediated therapy for SCA6
871 blocks IRES-driven translation of the CACNA1A second cistron. Sci Transl Med *8*, 347ra394.
872 Neely, A., and Hidalgo, P. (2014). Structure-function of proteins interacting with the alpha1 pore-forming
873 subunit of high-voltage-activated calcium channels. Front Physiol *5*, 209.
874 Raymond, C.R. (2007). LTP forms 1, 2 and 3: different mechanisms for the "long" in long-term
875 potentiation. Trends Neurosci *30*, 167-175.
876 Rodan, L.H., Spillmann, R.C., Kurata, H.T., Lamothe, S.M., Maghera, J., Jamra, R.A., Alkelai, A.,
877 Antonarakis, S.E., Atallah, I., Bar-Yosef, O.*, et al.* (2021). Phenotypic expansion of CACNA1C-associated
878 disorders to include isolated neurological manifestations. Genet Med *23*, 1922-1932.
879 Ruiz, A., Matute, C., and Alberdi, E. (2009). Endoplasmic reticulum Ca(2+) release through ryanodine and
880 IP(3) receptors contributes to neuronal excitotoxicity. Cell Calcium *46*, 273-281.

881 Rzhepetskyy, Y., Lazniewska, J., Blesneac, I., Pamphlett, R., and Weiss, N. (2016). CACNA1H missense
882 mutations associated with amyotrophic lateral sclerosis alter Cav3.2 T-type calcium channel activity and
883 reticular thalamic neuron firing. Channels (Austin) *10*, 466-477.
884 Sharma, R.P., Tun, N., and Grayson, D.R. (2008). Depolarization induces downregulation of DNMT1 and
885 DNMT3a in primary cortical cultures. Epigenetics *3*, 74-80.
886 Singh, A., Hamedinger, D., Hoda, J.C., Gebhart, M., Koschak, A., Romanin, C., and Striessnig, J. (2006). C-
887 terminal modulator controls Ca2+-dependent gating of Ca(v)1.4 L-type Ca2+ channels. Nat Neurosci *9*,
888 1108-1116.
889 Souza, I.A., Gandini, M.A., Wan, M.M., and Zamponi, G.W. (2016). Two heterozygous Cav3.2 channel
890 mutations in a pediatric chronic pain patient: recording condition-dependent biophysical effects.
891 Pflugers Arch *468*, 635-642.
892 Splawski, I., Timothy, K.W., Sharpe, L.M., Decher, N., Kumar, P., Bloise, R., Napolitano, C., Schwartz, P.J.,
893 Joseph, R.M., Condouris, K.*, et al.* (2004). Ca(V)1.2 calcium channel dysfunction causes a multisystem
894 disorder including arrhythmia and autism. Cell *119*, 19-31.
895 Splawski, I., Yoo, D.S., Stotz, S.C., Cherry, A., Clapham, D.E., and Keating, M.T. (2006). CACNA1H
896 mutations in autism spectrum disorders. J Biol Chem *281*, 22085-22091.
897 Spriggs, K.A., Cobbold, L.C., Jopling, C.L., Cooper, R.E., Wilson, L.A., Stoneley, M., Coldwell, M.J., Poncet,
898 D., Shen, Y.C., Morley, S.J.*, et al.* (2009). Canonical initiation factor requirements of the Myc family of
899 internal ribosome entry segments. Mol Cell Biol *29*, 1565-1574.
900 Stenoien, D.L., Nye, A.C., Mancini, M.G., Patel, K., Dutertre, M., O'Malley, B.W., Smith, C.L., Belmont,
901 A.S., and Mancini, M.A. (2001). Ligand-mediated assembly and real-time cellular dynamics of estrogen
902 receptor alpha-coactivator complexes in living cells. Mol Cell Biol *21*, 4404-4412.
903 Stringer, R.N., Jurkovicova-Tarabova, B., Huang, S., Haji-Ghassemi, O., Idoux, R., Liashenko, A., Souza,
904 I.A., Rzhepetskyy, Y., Lacinova, L., Van Petegem, F.*, et al.* (2020). A rare CACNA1H variant associated with
905 amyotrophic lateral sclerosis causes complete loss of Cav3.2 T-type channel activity. Mol Brain *13*, 33.
906 Wahl-Schott, C., Baumann, L., Cuny, H., Eckert, C., Griessmeier, K., and Biel, M. (2006). Switching off
907 calcium-dependent inactivation in L-type calcium channels by an autoinhibitory domain. Proc Natl Acad
908 Sci U S A *103*, 15657-15662.
909 Weiss, J.H., Hartley, D.M., Koh, J., and Choi, D.W. (1990). The calcium channel blocker nifedipine
910 attenuates slow excitatory amino acid neurotoxicity. Science *247*, 1474-1477.
911 Wheeler, D.B., Randall, A., and Tsien, R.W. (1994). Roles of N-type and Q-type Ca2+ channels in
912 supporting hippocampal synaptic transmission. Science *264*, 107-111.
913 Wheeler, D.G., Barrett, C.F., Groth, R.D., Safa, P., and Tsien, R.W. (2008). CaMKII locally encodes L-type
914 channel activity to signal to nuclear CREB in excitation-transcription coupling. J Cell Biol *183*, 849-863.
915 Wheeler, D.G., Groth, R.D., Ma, H., Barrett, C.F., Owen, S.F., Safa, P., and Tsien, R.W. (2012). Ca(V)1 and
916 Ca(V)2 channels engage distinct modes of Ca(2+) signaling to control CREB-dependent gene expression.
917 Cell *149*, 1112-1124.
918 Wong, F.K., Nath, A.R., Chen, R.H., Gardezi, S.R., Li, Q., and Stanley, E.F. (2014). Synaptic vesicle
919 tethering and the CaV2.2 distal C-terminal. Front Cell Neurosci *8*, 71.
920 Wu, G.Y., Deisseroth, K., and Tsien, R.W. (2001). Activity-dependent CREB phosphorylation: convergence
921 of a fast, sensitive calmodulin kinase pathway and a slow, less sensitive mitogen-activated protein
922 kinase pathway. Proc Natl Acad Sci U S A *98*, 2808-2813.
923 Xie, C.X., Mattson, M.P., Lovell, M.A., and Yokel, R.A. (1996). Intraneuronal aluminum potentiates iron-
924 induced oxidative stress in cultured rat hippocampal neurons. Brain Res *743*, 271-277.
925 Yang, Y., Yu, Z., Geng, J., Liu, M., Liu, N., Li, P., Hong, W., Yue, S., Jiang, H., Ge, H.*, et al.* (2022). Cytosolic
926 peptides encoding Ca(V)1 C-termini downregulate the calcium channel activity-neuritogenesis coupling.
927 Commun Biol *5*, 484.

928 Zhang, L.N., Wang, Q., Xian, X.H., Qi, J., Liu, L.Z., and Li, W.B. (2019). Astrocytes enhance the tolerance of
929 rat cortical neurons to glutamate excitotoxicity. Mol Med Rep *19*, 1521-1528.

930

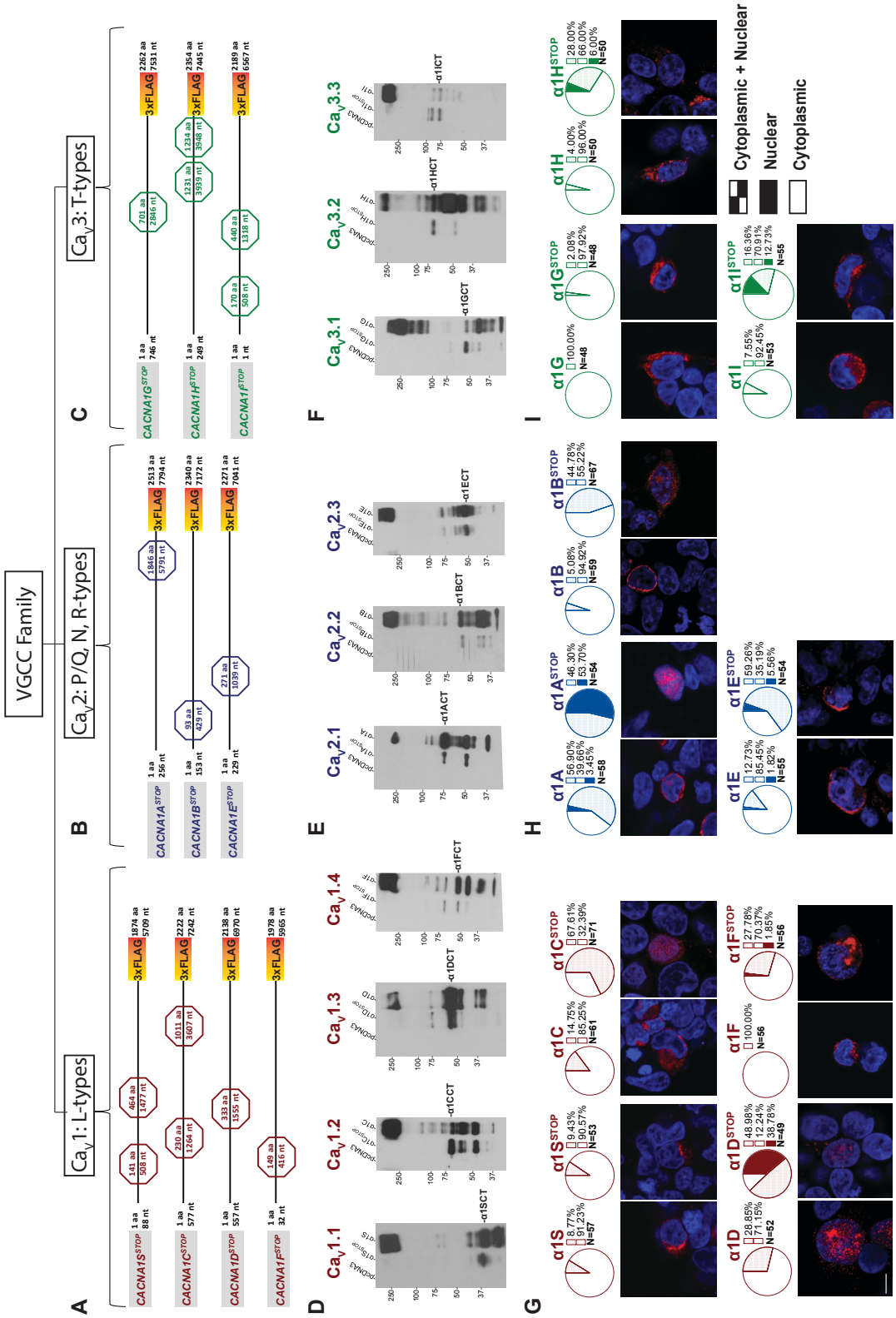

Figure 1. The VGCC gene family is bicistronic with C-terminal secondary proteins generated by all ten members and Subcellular localization of C-terminal secondary proteins expressed by ten VGCC cDNAs. See also Figure S1.

(A) Schematic representation of L type VGCC- *CACNA1S*, *CACNA1C*, *CACNA1D*, and *CACNA1F* -with STOP codon constructs.

(B) Schematic representation of P/Q, N, R type VGCC- *CACNA1A*, *CACNA1B*, and *CACNA1E* -with STOP codon constructs.

(C) Schematic representation of T type VGCC- *CACNA1G*, *CACNA1H*, and *CACNA1I* -with STOP codon constructs.

(D, E, and F) Western blot analysis of C-terminally 3XFLAG-tagged L type (D), P/Q, N, R type (E), and T type (F) VGCCs showing a secondary protein product detected by 3XFLAG antibody, that is produced independently of the full-length channel (FL). Secondary products ~37-85 kDa were observed in both full length and STOP code conditions, while the primary VGCC alpha subunits (~250 kDa) were only observed in FL conditions. Ca_V1 sub-family (D), Ca_V2 sub-family (E), Ca_V3 sub-family (F).

(G, H, and I) Representative confocal images of HEK293T cells transfected with either FL α1 VGCC subunit or STOP construct cDNA tagged with 3XFLAG (A, B, and C) and corresponding pie charts showing cellular compartment quantification of fluorescent signal for FL and STOP constructs in the Ca_V1 family (G), Ca_V2 family (H), and Ca_V3 family (I). Number of cells used for each quantification is shown. Scale bar (G, lower left) = 10 microns.

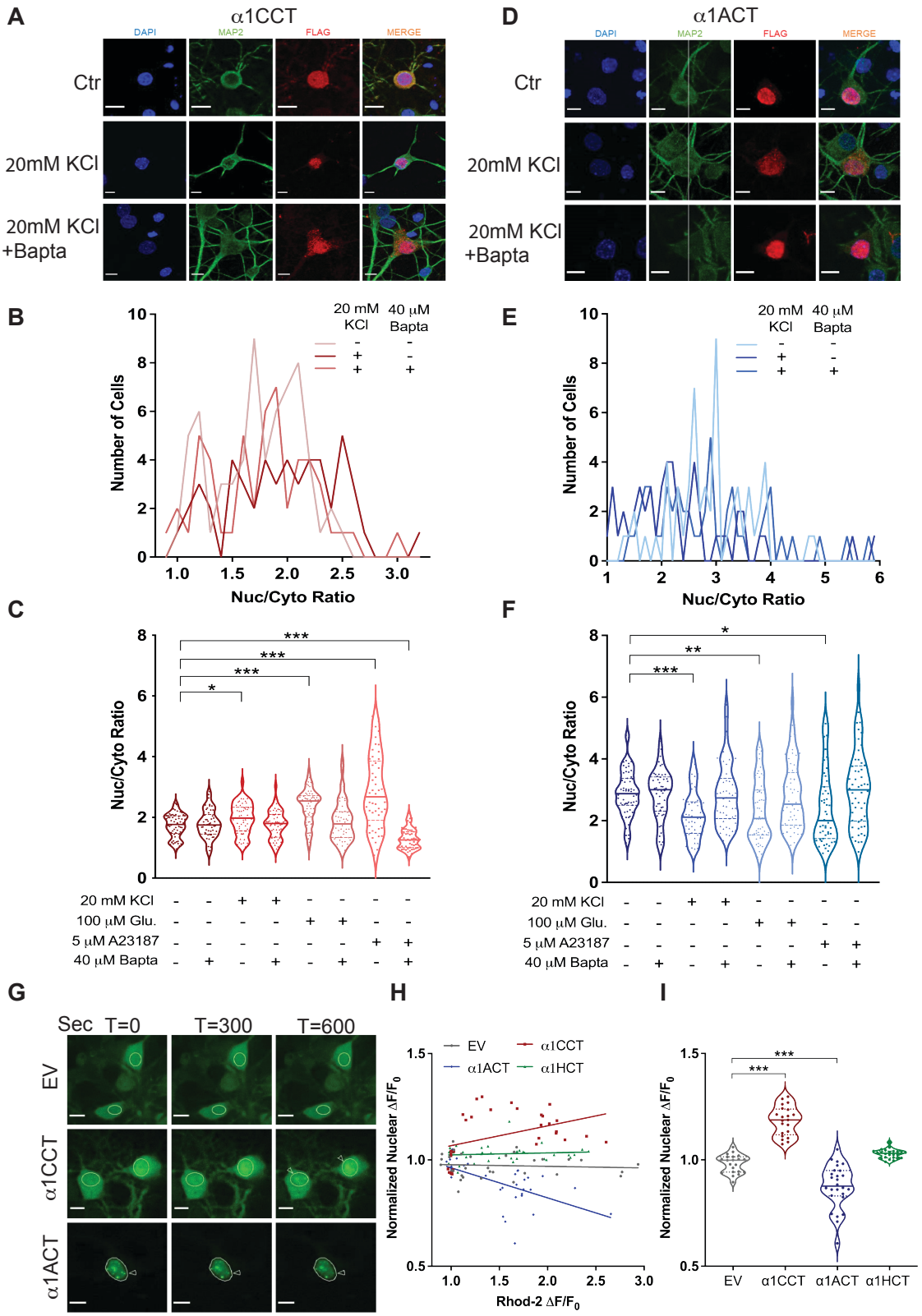

Figure 2. α1CCT and α1ACT translocate to or from the nucleus in response to elevated intracellular calcium. See also Figure S2.

(A) Representative images of fixed rat cortical neurons transfected with α1CCT mRNA and treated with 20mM KCl with or without BAPTA-AM. Fixed neurons were stained with DAPI (blue), MAP2 antibody(green), and 3XFLAG antibody (red). Scale bars = 10 microns.

(B) Quantification of nuclear/cytosolic fluorescence signal of rat cortical neurons transfected with α1CCT mRNA with 20mM KCl with or without BAPTA-AM.

(C) Quantification of nuclear/cytosolic fluorescence signal of rat cortical neurons transfected with α1CCT mRNA with different treatments.

(D) Representative images of fixed rat cortical neurons transfected with α1ACT mRNA and treated with 20mM KCl with or without BAPTA-AM. Fixed neurons were stained with DAPI (blue), MAP2 antibody (green), and 3XFLAG antibody (red). Scale bars = 10 microns.

(E) Quantification of nuclear/cytoplasmic fluorescence signal of rat cortical neurons transfected with α1ACT mRNA with 20mM KCl with or without BAPTA-AM.

(F) Quantification of nuclear/cytosolic fluorescence signal of rat cortical neurons transfected with α1ACT mRNA with different treatments.

(G) Representative live-cell images of rat cortical neurons infected with AAV9-EmGFP, AAV9-α1CCT-EmGFP, or AAV9- α1ACT-EmGFP virus at T = 0 seconds, T = 300 seconds, or T = 600 seconds post-glutamate uncaging. Circles denote the nucleus. Arrows denote putative nuclear speckle formation (α1CCT) or dissipation (α1ACT). Scale bars = 10 microns. Glutamate uncaging occurred at T = 15s with two 10ms pulses of 405 nm light. Images were collected every 3s for 10 minutes total.

(H) Graph depicting intracellular calcium spike (as measured by Rhod2 $\Delta F/F_0$) versus neuronal nuclear fluorescence change at T = 600s ($\Delta F/F_0$) for EmGFP, α1CCT, α1ACT, and α1HCT infected neurons (N > 30 cells for each condition)

(I) Normalized nuclear fluorescence $\Delta F/F_0$ for EmGFP, α1CCT, α1ACT, and α1HCT infected neurons at T=600s post-glutamate uncaging (N > 30 cells per condition, *$p<0.05$, **$p<0.01$, ***$p<0.001$).

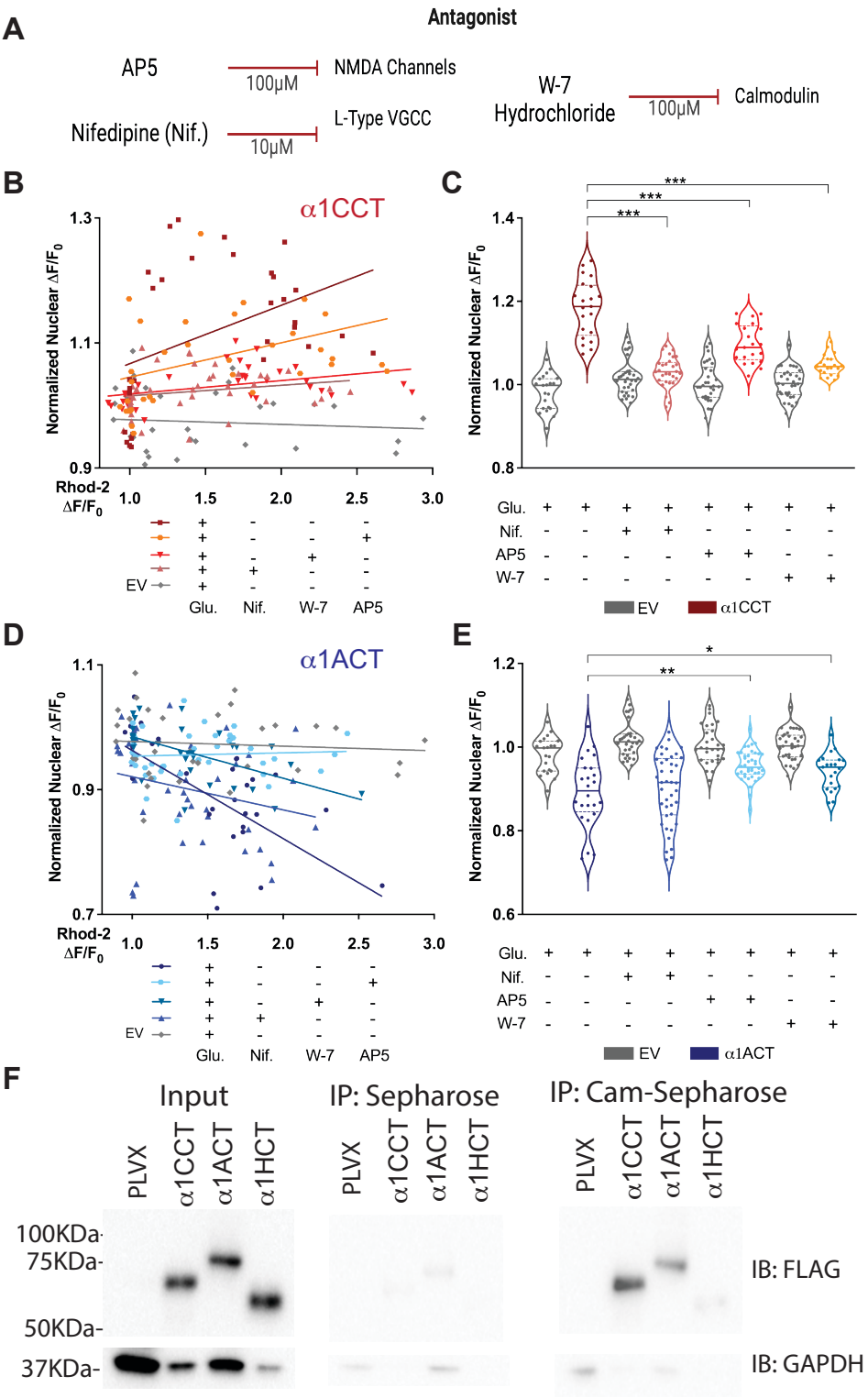

Figure 3. Nuclear translocation of α1CCT and α1ACT is coupled to calcium signaling through L-type VGCCs or NMDA receptors and calmodulin. See also Figure S3.

(A) The calcium-channel antagonists used in conjunction with live-neuron glutamate uncaging.

(B) Graph showing the comparison of α1CCT nuclear translocation following glutamate uncaging in the presence of L-type calcium channel antagonist (nifedipine), NMDA receptor antagonist (AP5), or calmodulin antagonist (W-7 hydrochloride). Negative control (-Glu) refer to Figure S2.

(C) Quantification of normalized nuclear $\Delta F/F_0$ at T = 600 seconds for α1CCT treatment conditions.

(D) Graph showing the comparison of α1ACT nuclear translocation following glutamate uncaging in the presence of nifedipine, AP5, or W-7. Negative control (-Glu) refer to Figure S2.

(E) Quantification of normalized nuclear $\Delta F/F_0$ at T = 600 seconds for α1ACT treatment conditions.

(F) Input samples showing 3XFLAG-tagged α1CCT, α1ACT, and α1HCT expression in lysates from H293T cell transfected with pLVX (control), α1CCT, α1ACT, and α1HCT. Immunoblotting (IB) was performed with anti-3XFLAG antibody, and anti-GAPDH antibody as loading control. Negative control immunoprecipitation (IP) using unconjugated Sepharose beads, showing minimal non-specific binding of α1CCT, α1ACT, and α1HCT. Calmodulin-Sepharose IP demonstrating specific interaction of α1CCT and α1ACT with calmodulin. 3XFLAG-tagged proteins were detected in the pull-down fractions, confirming their binding to calmodulin.

N > 30 cells per condition, *$p<0.05$, **$p<0.01$, ***$p<0.001$.

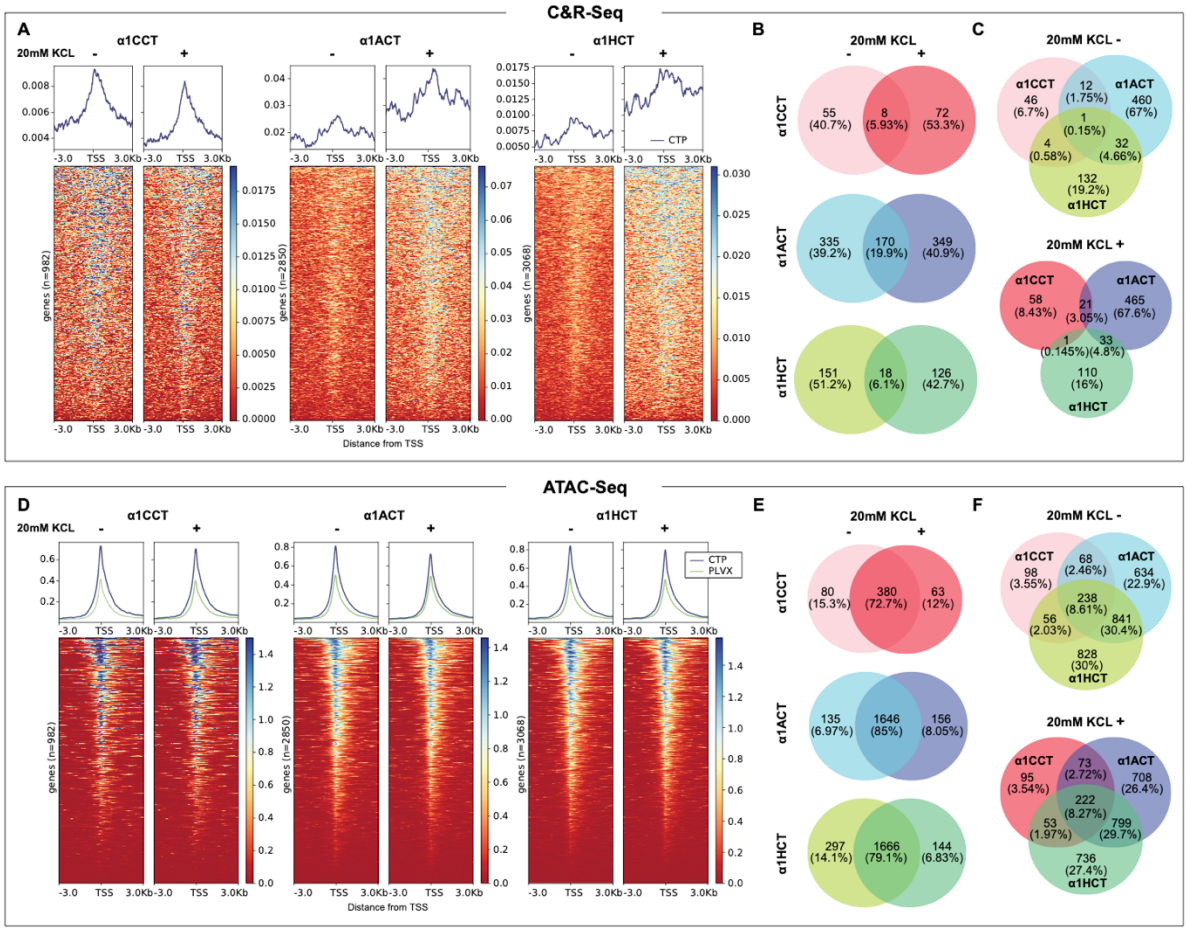

Figure 4. α1CCT, α1ACT, and α1HCT bind to genomic DNA in a Ca^{2+}-dependent manner and alter chromatin accessibility independently of Ca^{2+} influx. See also Figure S4.

(A) α1CCT, α1ACT, and α1HCT putative DNA binding profile within ±3000bp relative to the transcription start site (TSS) of DEGs in both resting and depolarized cells. Heatmaps display the CUT&RUN signal intensity across target sites, with corresponding aggregate signal profiles (above). The intensity score was derived from the sequencing read coverage.

(B) Venn diagrams indicate the limited overlaps in DEGs-associated genomic binding sites in resting and depolarized cells for α1CCT, α1ACT, and α1HCT.

(C) Venn diagrams indicate overlaps in DEGs-associated genomic binding sites for α1CCT, α1ACT, and α1HCT in resting and depolarized cells, highlighting the unique binding patterns among the three CTPs.

(D) α1CCT, α1ACT, and α1HCT affects chromatin accessibility distribution ±3000bp TSS in resting and depolarized cells. Heatmaps show chromatin accessibility as measured by ATAC-seq, with aggregate signal profiles, pLVX is control, shown in green (above).

(E) Venn diagrams indicate the prominent overlaps in chromatin accessibility of DEG-regulatory regions between resting and depolarized cells induced by α1CCT, α1ACT, and α1HCT.

(F) Venn diagrams illustrate the overlap in chromatin accessibility of chromatin-accessible DEG-regulatory regions among α1CCT, α1ACT, and α1HCT in resting and depolarized cells. Shared and unique regions emphasize their differential impacts on chromatin structure.

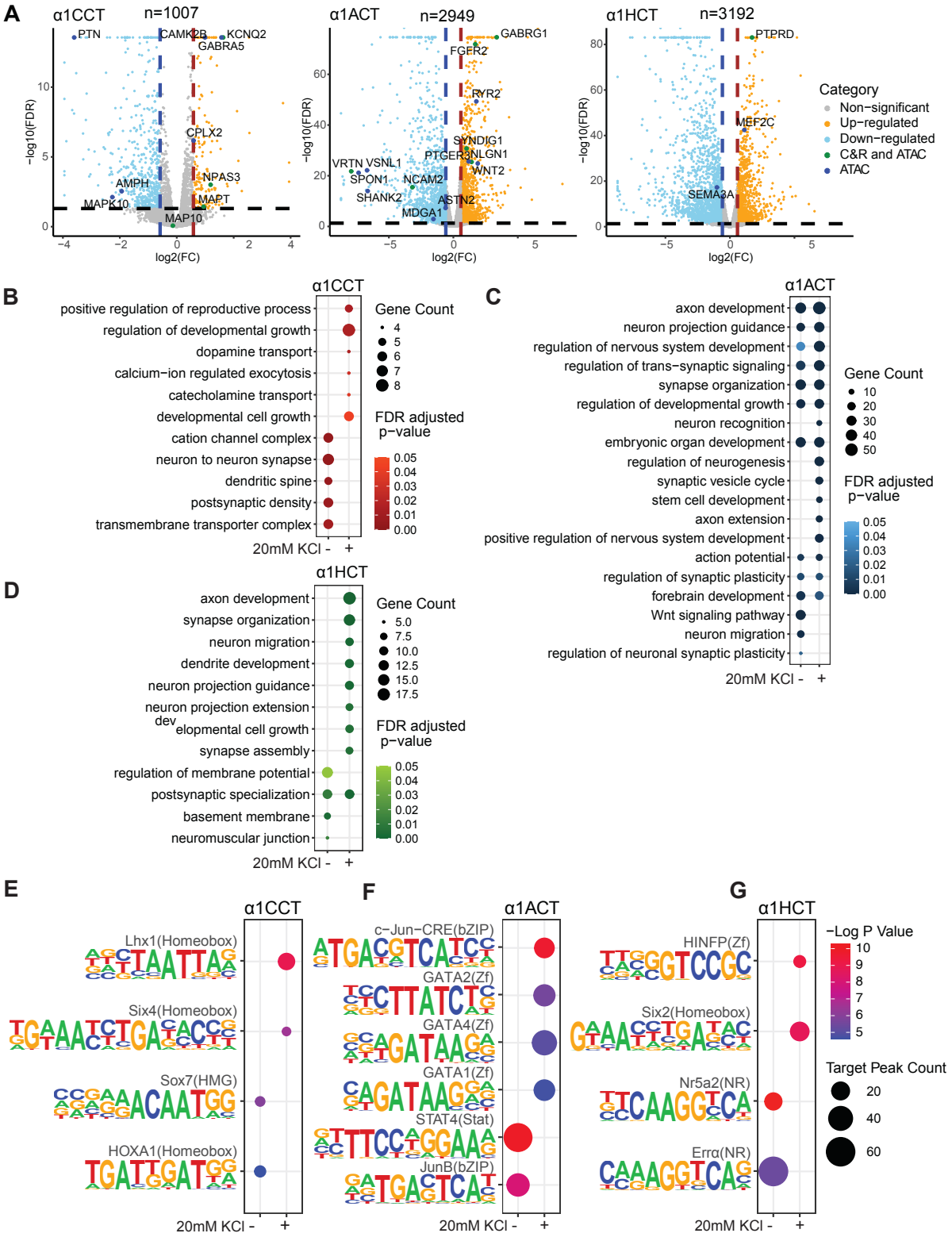

Figure 5. α1CCT, α1ACT, and α1HCT promote a genetic neural differentiation program in hNPCs by binding to DNA in a Ca^{2+} dependent manner. See also Figure S5.

(A) Volcano plots of RNA-seq DEGs, the qRT-PCR-verified DEGs are highlighted as two categories, either with regulatory binding sites from both CUT&RUN-seq and ATAC-seq, or from ATAC-seq only.

(B) Distinct enriched GO terms for RNA-seq DEGs directly regulated by α1CCT, inferred by CUT&RUN-seq, in hNPCs stably expressing α1CCT, with or without 20 mM KCl treatment.

(C) Top enriched GO terms for RNA-seq DEGs directly regulated by α1ACT, inferred by CUT&RUN-seq, in hNPCs stably expressing α1ACT, with or without 20 mM KCl treatment.

(D) Distinct enriched GO terms for RNA-seq DEGs directly regulated by α1HCT, inferred by CUT&RUN-seq, in hNPCs stably expressing α1HCT, with or without 20 mM KCl treatment.

(E, F, and G) Distinct enriched DNA motifs from CUT&RUN-seq binding sites with an RNA-seq DEG annotation, for α1CCT (E), α1ACT (F), and α1HCT (G) with and without 20mM KCl treatment.

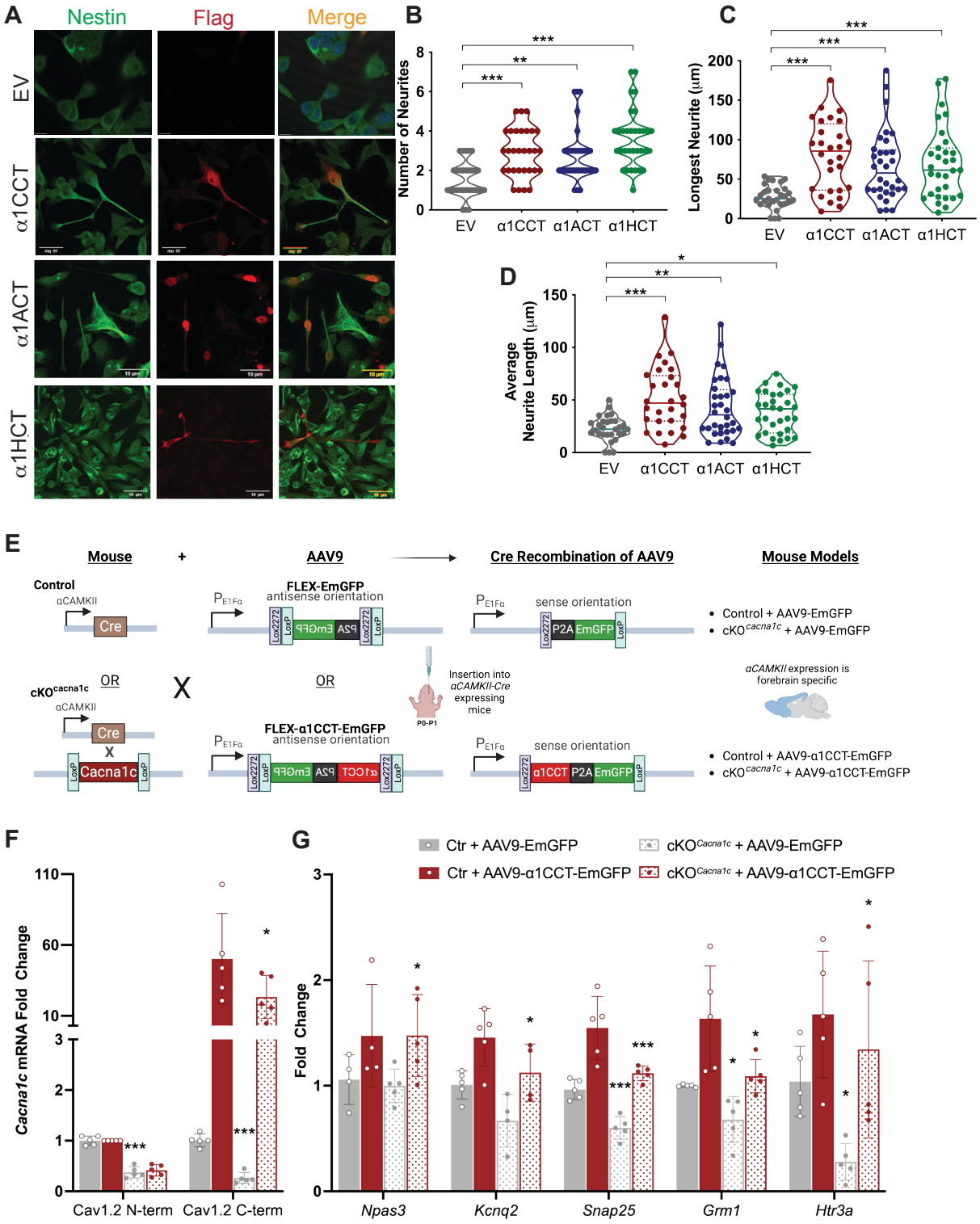

Figure 6. α1CCT, α1ACT, and α1HCT promote neurite outgrowth in hNPCs, and α1CCT restores expression of critical neuronal genes in a conditional forebrain *Cacna1c* knockout mouse model.

(A) Representative images of hNPCs stably expressing C-terminal 3XFLAG tag-labeled α1CCT, α1ACT, or α1HCT co-stained with antibodies directed against the hNPC marker Nestin (green) or 3XFLAG (red).

(B, C, and D) Quantification of neurites per cell, longest neurite per cell, and average neurite length ($n > 30$ cells, *$p<0.05$, **$p<0.01$, ***$p<0.001$).

(E) Schematic diagram showing the AAV-FLEX-EmGFP or AAV-FLEX-α1CCT-EmGFP viral vectors used for *in vivo* injections and the derived mouse models.

(F) Validation qRT-PCR analysis of *Cacna1c* knockout and α1CCT re-expression using primers directed at the 5' or 3' ends of the gene, respectively.

(G) qRT-PCR analysis of selected upregulated and downregulated DEGs identified through RNA-seq in microdissected mouse forebrain tissue

N = 4-5 mice per condition, *$p<0.05$, **$p<0.01$, ***$p<0.001$